Depicting Transcranial Magnetic Stimulation from a Neuronal Perspective

Dissertation

zur Erlangung des Grades eines
Doktors der Naturwissenschaften

der Mathematisch-Naturwissenschaftlichen Fakultät
und
der Medizinischen Fakultät
der Eberhard-Karls-Universität Tübingen

vorgelegt
von

Bingshuo Li
aus Baoding, Hebei, China

2022

Tag der mündlichen Prüfung: 18.11.2022

Dekan der Math.-Nat. Fakultät: Prof. Dr. Thilo Stehle
Dekan der Medizinischen Fakultät: Prof. Dr. Bernd Pichler

1. Berichterstatter: Prof. Dr. Cornelius Schwarz
2. Berichterstatter: Prof. Dr. Klaus Scheffler

Prüfungskommission: Prof. Dr. Andreas Bartels
Prof. Dr. Cornelius Schwarz
Prof. Dr. Martin Giese
Prof. Dr. Klaus Scheffler

Erklärung

Ich erkläre, dass ich die zur Promotion eingereichte Arbeit mit dem Titel:

„Depicting Transcranial Magnetic Stimulation from a Neuronal Perspective“

selbständig verfasst, nur die angegebenen Quellen und Hilfsmittel benutzt und wörtlich oder inhaltlich übernommene Stellen als solche gekennzeichnet habe. Ich versichere an Eides statt, dass diese Angaben wahr sind und dass ich nichts verschwiegen habe. Mir ist bekannt, dass die falsche Abgabe einer Versicherung an Eides statt mit Freiheitsstrafe bis zu drei Jahren oder mit Geldstrafe bestraft wird.

Tübingen, den 18.11.2022

Datum / Date

Unterschrift / Signature

TABLE OF CONTENTS

1. General introduction 8

1.1 Mechanistic insights from human studies.....10
1.2 Mechanistic insights from animal studies 13
1.3 Outline of this doctoral work.....16

2. Development of an experimental platform for concurrent TMS-EEP studies in laboratory rodents 18

2.1 Introduction.....19
2.2 Results.....20
2.3 Discussion 33
2.4 Materials and Methods.....36
2.5 Contributions.....40
2.6 Acknowledgements.....41
2.7 Supplementary Information 42

3. Characterizing the dynamics of neuronal activities in M1 evoked by a monophasic single-pulse TMS 45

3.1 Introduction.....46
3.2 Results.....46
3.3 Discussion 51
3.4 Materials and Methods.....58
3.5 Contributions.....61
3.6 Supplementary Information 63

4. Investigating the circuit mechanism underlying TMS-evoked intermediate excitation.....66

4.1 Introduction 67
4.2 Results 72
4.3 Discussion 77
4.4 Materials and Methods 81
4.5 Contributions 84
4.6 Supplementary Information 86

5. Conclusion 87
6. References 93
7. Acknowledgement 109

LIST OF ABBREVIATIONS

BG	Basal ganglia
BZ	Basal ganglia input zone of motor thalamus
CB	Calbindin
CBGTC	Cortico-basal ganglia-thalamo-cortical
CCTC	Cortico-cerebello-thalamo-cortical
cTBS	Continuous theta burst stimulation
CZ	Cerebellum input zone of motor thalamus
DBS	Deep brain stimulation
DCN	Deep cerebellar nuclei
EEG	Electroencephalography
EEP	Extracellular electrophysiology
emf	Electromotive force
EMG	Electromyogram
fMRI	Functional magnetic resonance imaging
FR	Firing rate
$GABA_AR$	Gamma-aminobutyric acid type A receptor
$GABA_BR$	Gamma-aminobutyric acid type B receptor
GPi	Internal globus pallidus
i.p.	Intraperitoneal
ICMS	Intracortical microstimulation
IT	Intratelencephalic
iTBS	Intermittent theta burst stimulation
ML	Medial to lateral
MSO	Maximum stimulator output

mspTMS	Monophasic single-pulse TMS
MT	Motor threshold
MUAP	Motor unit action potentials
M1	Primary motor cortex
PA	Posterior to the anterior
PC	Paracentral nucleus
PD	Parkinson's disease
PET	Positron emission tomography
PO	Posterior nucleus
PSTH	Peristimulus time histogram
PV	Parvalbumin
SICF	Short interval intracortical facilitation
SNr	Substantia nigra pars reticulata
SSSW	Solid-state analog switch
STN	Subthalamic nucleus
SubV	Ventral submedius nucleus
TBS	Theta burst stimulation
TMS	Transcranial magnetic stimulation
VA	Ventral anterior thalamic nucleus
VL	Ventral lateral thalamic nucleus
VM	Ventral medial thalamic nucleus
VPM	Ventral posteromedial nucleus
V1	Primary visual cortex

1. General introduction

The physical basis of transcranial magnetic stimulation (TMS) resides on Faraday's electromagnetic induction principle. A rapidly changing magnetic field, generated by a large alternating current pulse in a coil, penetrates non-invasively the skin and the skull of a human head and induces electric currents in the brain that stimulate various excitable neuronal elements. Since its introduction (Barker et al., 1985), TMS has gained considerable popularity in neuroscience, neurology, and psychiatry. For its non-invasiveness and its capability of activating or modulating cortical neuronal populations, TMS has produced widespread research applications in areas such as perception and cognition (Walsh and Cowey, 2000), motor control (Reis et al., 2008), neuroplasticity (Cohen et al., 1998), as well as clinical applications in the management of many neurological and psychiatric disorders (Lefaucheur et al., 2014).

Despite its rapidly expanding use, the neurophysiology of TMS remains poorly understood. The non-invasive nature of TMS precludes the direct investigation of TMS-evoked neuronal activities in humans, and an array of technical challenges render the investigation in laboratory animals extremely difficult. Most of our current understanding of the physiology of TMS is based on indirect evidence from recordings of TMS-evoked readouts of the brain such as motor-evoked potential (MEP) and corticospinal volley. Although multiple lines of indirect evidence support the use of TMS in multiple contexts (Chung et al., 2015; Di Lazzaro et al., 2008; Suppa et al., 2016), our limited insight into the neurophysiology of TMS remains a bottleneck that impedes the

utilization and the development of TMS, blocking the exciting potential of this non-invasive brain stimulation tool.

In the following parts of this general introduction, I will provide a brief review of our current understanding of the neurophysiology of TMS obtained from human and animal studies, and subsequently, argue for the need of developing a research platform on which TMS-evoked neuronal activities can be studied in the brain in laboratory animals *in vivo* in real time.

1.1 Mechanistic insights from human studies

It has been well-established that a TMS pulse delivered to the primary motor cortex (M1) can elicit a muscle twitch (Barker et al., 1985; Hess et al., 1987) that can be quantified by electromyography (EMG) as MEP. It is believed that MEP is a result of direct and indirect activation of M1 layer V pyramidal neurons by TMS. This is supported by evidence from epidural corticospinal volley recordings in patients with spinal cord implants. A single TMS pulse over M1 with sufficient strength could evoke multiple descending corticospinal volleys termed direct (D-) and indirect (I-) waves, depending on their latency to the TMS stimulus (Di Lazzaro et al., 1998). The 2-2.6 ms latency of the D-wave, measured from the high cervical spinal cord, suggests the direct excitation of the layer V pyramidal neurons while the first indirect wave, the I1-wave, with a latency that is 1-1.2 ms longer than the D-wave, suggests the activation of layer V pyramidal neurons due to synaptic activation. The I1-wave is followed by late I-waves (I2, I3, etc.) that arrive at the recording site with a periodicity of 1.5 ms, suggesting repeated activation

of layer V pyramidal neurons by some type of recurrent network activity. The generation of late I-waves, but not I1-wave or D-wave, can be modulated by the gamma-aminobutyric acid type A receptor ($GABA_AR$) system, as drugs that enhance $GABA_AR$ function such as lorazepam can depress late I-waves (Di Lazzaro et al., 2000). This provides evidence that interneurons projecting onto layer V pyramidal neurons are involved in TMS-activation that gives rise to late I-wave. More complicated patterns of interactions were reported in studies that utilized paired-pulse TMS. A subthreshold conditioning pulse that by itself does not generate any corticospinal volley could, given an interstimulus interval (ISI) between 1 and 5 ms, depress late I-waves generated by a suprathreshold test pulse while leaving the I1-wave intact (Kujirai et al., 1993). This offers the insight that a TMS pulse not strong enough to activate layer V pyramidal neurons could nonetheless modulate interneurons directly or indirectly, affecting the generation of late I-waves. In another paired-pulse paradigm, a suprathreshold conditioning pulse that is given 100 ms prior to a test pulse could also selectively depress late I-waves (Nakamura et al., 1997) and such effect is sensitive to GABA type B receptor system ($GABA_BR$) manipulation (McDonnell et al., 2006). This finding supports the notion that the late, $GABA_BR$-mediated inhibition effect could be recruited by TMS. Several models of TMS-evoked cortical neuronal activities have been developed to account for these findings (Esser et al., 2005; Di Lazzaro and Ziemann, 2013; Rusu et al., 2014; Sakai et al., 1997; Ziemann and Rothwell, 2000) but all remain putative as methodological challenges obscure the direct observation of TMS-evoked neuronal activities in the cerebral cortex.

When applied repetitively, TMS is known to produce changes in cortical excitability that outlasts the duration of stimulation. Using the difference of MEP amplitude before and after repetitive stimulation as an index, it has been shown that low-frequency repetitive stimulation (1-3 Hz) and continuous theta burst stimulation (cTBS) induce a suppressive effect on MEP (Chen et al., 1997; Huang et al., 2005) while high-frequency repetitive stimulation (5-20 Hz) and intermittent theta burst stimulation (iTBS) lead to a faciliatory effect on MEP (Huang et al., 2005; Pascual-Leone et al., 1994). These effects are termed as either long-term potentiation (LTP) - like plasticity, or long-term depression (LTD) - like plasticity for their similarity to LTP and LTD from intracellular studies of synaptic plasticity (Malenka and Bear, 2004). Despite the apparent similarities between the classical synaptic LTP/LTD and the LTP-like/LTD-like plasticity in repetitive TMS (rTMS), the neurophysiological mechanisms of the latter remain elusive. Owing to its non-invasiveness and ability to induce plasticity, rTMS is being actively explored for the treatment of a wide range of neurological and psychiatric disorders. However, the effects of rTMS-based interventions remain highly heterogenous, ranging from no effects to small and short-lasting effects for certain patient populations (Lefaucheur et al., 2014). Such limited success, as argued by the leading experts of the field, is the result of TMS-based clinical application development greatly exceeding our understanding of its underlying neurobiological mechanisms (Wagner et al., 2007). This is a critical issue that needs be addressed in order to develop TMS-based therapeutic interventions that are more effective and durable.

In summary, on one hand, a set of TMS-evoked physiological phenomena have been established through human studies: we know a single TMS delivered to the motor cortex can evoke a series of corticospinal volleys and MEP; we know that a conditioning TMS pulse can modulate MEP or corticospinal volleys evoked by a later TMS pulse; we know that rTMS can induce LTP- or LTD-like changes, depending on the pattern of stimulus repetition; and we know that rTMS-based interventions have shown observable, albeit small and short-lasting, therapeutic effects for certain psychiatric and neurological disorders; on the other hand, the neurophysiological mechanisms of TMS remain poorly understood, and the development of TMS applications has largely been following the principle of trial-and-error. Therefore, a better understanding of how TMS interacts with neurons and neuronal circuits will undoubtedly facilitate the development of TMS applications by providing much-needed guidance from neurophysiology.

1.2 Mechanistic insights from animal studies

The core advantage of TMS over many other brain stimulation techniques is its non-invasiveness. However, the study of TMS-evoked neuronal activities with single-neuron resolution and millisecond precision requires invasive access to the brain. This conundrum naturally calls for a solution in the domain of animal research. However, the study of TMS neurophysiology using animal models has been difficult. This is a result of two technical constraints. First, due to its physical nature, TMS creates an extremely harsh electromagnetic environment for extracellular electrophysiology (EEP), the gold standard

for studying neuronal activities. A typical TMS pulse generates a transient alternating magnetic field with intensity in the order of 1 to 4 tesla (Wagner et al., 2007). This is far more than enough to cause strong interferences in a typical EEP recording system, leading to data loss lasting up to several hundreds of milliseconds that markedly obscures our investigation on the neuronal dynamics in the brain following TMS. The other technical constraint is the size of a TMS coil. Coils that are designed for routine stimulation in humans are too large for most laboratory animals. A typical human TMS coil measures between 9 to 18 cm in diameter (The Magstim Company Ltd., 2018), which is much larger than the brain of commonly used laboratory animals. Therefore, it is difficult to deliver focused stimulation in the brain of laboratory animals using TMS.

In a few studies, researchers conducted EEP recording in laboratory animals under TMS despite its heavy electromagnetic interference. Moliadze et al. (2003) reported that a single biphasic TMS pulse elicited distinct episodes of enhanced and suppressed spiking activities in the primary visual cortex (V1) of anesthetized cats. The facilitation occurred during the first 500 ms after TMS onset and it was followed by a period of suppression that lasted up to a few seconds. Other groups of researchers reported that a short train of TMS pulses (4 Hz for 2 s) elicited periods of long-lasting excitation (~1 min) and suppression (~ 5-10 min) (Allen et al., 2007), and TMS-evoked multi-unit spiking and local field potential (LFP) response patterns vary with brain state (Pasley et al., 2009). Despite their pioneering attempts, in the absence of technology that deals with the large electromagnetic

inference from TMS, these researchers all had to discard a significant amount of data (up to hundreds of milliseconds) after each TMS pulse, obscuring their view to the immediate neuronal response evoked by TMS. Furthermore, by connecting an animal to the EEP electronics and expose the resulted circuit to large fluctuating electrical and magnetic field, these researchers faced the risk of driving current into the brain through their recording electrodes, a risk that can severely confound the measurements of TMS-evoked neuronal activities.

Several groups adopted innovative methods to circumvent the problem of electromagnetic interference in EEP. Optical imaging such as voltage-sensitive dye (VSD) imaging and fluorescence imaging are immune to the electromagnetic interference resulted from TMS owing to the physical properties of light. In a VSD study in the V1 of anesthetized cats, it was found that a single TMS pulse elicited immediate excitation followed by long inhibition, and a subsequent 10 Hz pulse train delivered during inhibition increased cortical excitability (Kozyrev et al., 2014). Using a fluorescent calcium indicator and optical fiber imaging, Murphy et al. (2016) reported that TMS results in $GABA_BR$-mediated inhibition of sensory-evoked calcium activity in the apical dendrites of layer V pyramidal neurons in rats. These studies no doubt advanced our understanding of the physiology of TMS; however, they are limited by the coarse spatial or slow temporal resolution of these imaging methods, making them unable to reach the single-neuron and millisecond precision needed to decipher the intricate effects of TMS on individual neurons and their networks. Another way to circumvent the electromagnetic interference problem is to perform *ex vivo* study of

laboratory animals. Changes in an array of biochemical markers of neuronal activities, such as immediate early gene protein cFos and zif268, calcium binding proteins parvalbumin (PV) and calbindin D-28k (CB), have been investigated in the context of different rTMS protocols (Aydin-Abidin et al., 2008; Funke and Benali, 2010; Labedi et al., 2014; Mix et al., 2010). However, these investigations were seriously limited by their complete lack of temporal resolution and the low specificity of *ex vivo* biochemical markers in measuring the dynamics of TMS-evoked neuronal activities *in vivo*.

To conclude, animal studies of TMS conducted so far remain unsatisfactory in resolving the neurophysiological mechanisms underlying TMS. This is largely due to various methodological constraints: data loss in EEP results from the electromagnetic interference; inadvertent charge injection in EEP that confounds the measurement results; poor spatiotemporal resolution of optical imaging studies; and the lack of temporal resolution and the low *in vivo* specificity of *ex vivo* studies. The absence of an experimental platform on which TMS can be studied *in vivo* using laboratory animals at the level of neurons and their microcircuits with high spatiotemporal resolution, strongly impedes the research and development of TMS-based therapeutic applications.

1.3 Outline of this doctoral work

With these technical limitations and gaps in scientific knowledge in mind, I began the endeavor to develop an *in vivo* EEP-based animal experimental platform for TMS. The following chapters of this

dissertation are organized by three interconnected topics. The second chapter is dedicated to the technical development of a research platform that allows faithful concurrent TMS and EEP recording in laboratory rodents. Building on this methodology, the third chapter focuses on characterizing the dynamics of neuronal activities in M1 evoked by a monophasic single-pulse TMS (mspTMS) that triggers unilateral MEPs in the forearm. Bringing the investigation further, the fourth chapter explores the mechanism of TMS-evoked intermediate excitation, a period of synaptic-mediated excitatory neuronal activities in M1 triggered by TMS, in the cortico-basal ganglia-thalamo-cortical (CBGTC) and the cortico-cerebello-thalamo-cortical (CCTC) loop. Finally, the fifth chapter summarizes the results from this work, discusses their limitations and implications, and proposes future research.

2. Development of an experimental platform for concurrent TMS-EEP studies in laboratory rodents

This chapter is adapted from the following publication:

Li, B., Virtanen, J.P., Oeltermann, A., Schwarz, C., Giese, M.A., Ziemann, U., and Benali, A. (2017). Lifting the veil on the dynamics of neuronal activities evoked by transcranial magnetic stimulation. *eLife*, 6, 1–22.

2.1 Introduction

The core problem in concurrent TMS and EEP lies at the harsh electromagnetic environment that TMS creates. Using an extremely fast current pulse peaking at several kiloamperes to create a tesla-level magnetic field, TMS creates a series of problems in the electronics for EEP. First, just as TMS can induce an electromotive force (emf) that drives currents in biological tissues for stimulation, TMS can also induce an emf in the circuits of EEP electronics. Such unwanted emf causes strong interference in the normal functioning of the electronics. In the "best" case, it results in artifacts in EEP recordings that may last up to several hundreds of milliseconds. In the worst case, it causes permanent damages to the electronics. Second, the kiloamperes of current that runs inside of a TMS coil emits a strong electrical field that can be coupled to the circuits of EEP electronics, giving rise to another source of artifacts and possible damages. Third, TMS also causes vibrations in its vicinity through magnetic force or sound. Such vibrations can lead to the displacement of electrodes and again artifacts in EEP. Forth, as TMS induces an emf in the circuits of EEP electronics, such emf might be high enough to drive current through the high-impedance components of the EEP electronics, resulting in electrical stimulation at the tip of recording electrodes inserted into the brain.

Therefore, the design of an experimental platform for concurrent TMS and EEP must adequately address these technical challenges. In addition, to ensure the easy adoption by the neuroscience community, an ideal experimental platform shall also be simple to implement,

compatible with standard TMS devices, and applicable to a wide range of laboratory animal models.

With these considerations in mind, I took the initiative in developing a novel experimental platform for TMS-EEP that is suitable for, but not limited to, laboratory rodents, which are widely accessible and offer a rich repertoire of experimental techniques including transgenic and optogenetic tools. The platform is fully compatible with the standard TMS systems and allows the recording of neuronal activities 0.8–1 ms after the onset of various types of TMS stimuli by attenuating artifacts resulting from magnetic induction, electric field coupling, and vibration. In addition, the platform also includes a dedicated mechanism to minimize and monitor the amount of TMS-driven inadvertent charge injection into the neural tissue, a major possible confound in any TMS-EEP study. In the following sections of this chapter, I will describe the technical details of this platform and demonstrate its performance by presenting data recorded in anesthetized rats under various strong TMS stimuli ranging from single-pulse to theta-burst stimulation.

2.2 Results

2.2.1 Attenuation of the induction artifact

The induction artifact (Figure 2.1, period indicated in blue) is created as coil-generated rapid magnetic flux change induces voltages within loops formed along an EEP recording assembly. Owing to the large rate of flux change, the induction artifact, if transmitted to the high-

gain and filter stages of an EEP amplifier, can easily lead to signal saturation and data loss (Figure 2.1 inset). To address this, we developed a gated multi-stage TMS-EEP amplifier (Figure 2.2). It consists of a differential preamplifier (Pamp) stage of gain 4 and a filter-amplifier (Famp) stage of gain 500, separated by an ultra-low capacitance/charge injection solid-state analog switch (SSSW) controlled by optically coupled digital signal synchronized to TMS. The components of the amplifier were chosen to provide the optimal balance between voltage and current noise with the source impedance of EEP microelectrodes. The Pamp stage must be able to maintain its high impedance character when being perturbed by TMS. Failing to do so will result in excessive induction current in the input wires that leads to electrical stimulation of the brain. In our design, the electronic components and supply voltage of the Pamp stage were chosen so it can tolerate ±7.9 V input during TMS. Due to its high-gain and filters, the Famp stage must be protected from TMS by SSSW that grounds the input to Famp for a user-defined time interval around TMS onset (e.g. from 0.2 ms pre- to 0.8 ms post-TMS). The SSSW was strategically placed behind the input capacitor of a high-pass filter of the Famp so that the input capacitor is preconditioned to any DC bias in the

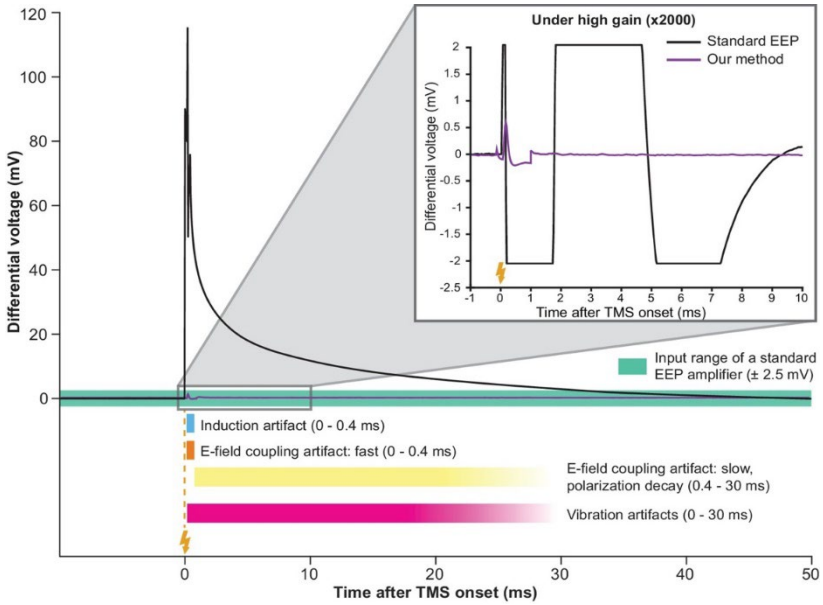

Figure 2.1: Simultaneous TMS-EEP recording requires artifact attenuation in multiple dimensions. The full waveform of a TMS artifact recorded differentially under low-gain (x4) using a high impedance amplifier. The artifact consists of a series of sharp deflections (induction and fast E-field coupling artifacts) and a long tail (polarization decay artifact resulted from E-field coupling). The slow polarization decay artifact renders the signal out of range (indicated by the green area) until ca. 30 ms post-TMS in a standard EEP system. Vibration artifacts (see Figure 2.4) are not visible here due to low amplification. The inset shows that under high-gain (x2000) needed for EEP, TMS artifacts lead to long signal saturation in a standard EEP system (bandpass 300–5000 Hz) while producing negligible interference in our method. Lightning symbol, TMS onset (at 0 ms). E-field, electric field.

microelectrodes before the end of the grounding period. To minimize ground bounce and to reduce ground loop, the external digital signal that controls SSSW is connected to the amplifier circuit through an optocoupler (OC). In addition, to protect the amplifier circuit from TMS-induced fields, the circuit board of the amplifier is mounted inside a 1.5 mm-thick grounded aluminum enclosure. The Pamp, as well as DC-DC converters, is housed inside a metal shield for additional protection.

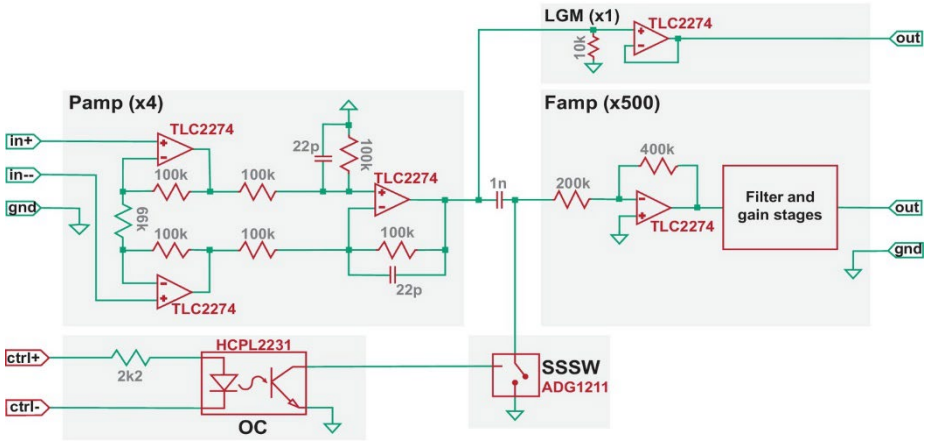

Figure 2.2: Simplified circuit diagram of the TMS-EEP amplifier. Model numbers of the most critical electronic components are noted in red, the values of certain elementary components are noted in grey (units: ohm for resistor; farad for capacitor), and the amplification factor for each stage is indicated in parenthesis. Pamp, pre-amplifier stage; Famp, filter-amplifier stage; OC, optocoupler; SSSW, solid-state analog switch; LGM, low-gain monitoring channel.

Furthermore, to minimize artifacts from vibrations due to the loud click sound of TMS coils, solder contacts, instead of spring-loaded connectors, were used whenever possible, as well as polyphenylene sulfide film capacitors, since they do not generate piezoelectric voltages from vibration. The default frequency response of the amplifier was set from 300 Hz (-3 dB) to 5 kHz (-6 dB), but the lower bound of the passband can be adjusted to 4 Hz as needed for different applications. A simplified circuit diagram of the amplifier, including the model number of its critical components, is shown in Figure 2.2.

2.2.2 Attenuation of electric field coupling artifacts

The coil-emitted electric field gives rise to another type of artifacts. When a TMS pulse is triggered, a large current driven by a kV-level

voltage pulse flows through the coil. Inadvertently, this process emits an electric field that injects a displacement current into the EEP recording assembly through capacitive coupling (Figure 2.3A). In a short time-interval (< 0.4 ms; Figure 2.1, period indicated in orange), as the coil current rapidly fluctuates, the displacement current generates a fast-changing artifact in EEP signal. In a long time-interval (tens of ms; Figure 2.1, period indicated in yellow), a decay-like artifact is observed as the displacement current polarizes the electrochemical double-layer of microelectrode tips and thereby generates a decaying waveform while the double-layer returns to its equilibrium potential. Depending on stimulation intensity, electrode impedance, and filter settings, the decay may persist with relatively high signal values for tens of milliseconds before re-entering the input range of a standard EEP amplifier (Figure 2.1, area indicated in green), contributing to an extended period of data loss. To address this problem, we developed an electrical shield for the TMS coil that substantially attenuates the coil-emitted electric field (Figure 2.3B). One important consideration in shield construction is that the amount of eddy current in the shield should remain low; otherwise, strong vibration or even magnetic attenuation may occur. Therefore, we applied a layer of weakly conducting material in shield construction and the resulted shield possesses an electrical resistance of 10 kΩ (see Materials and Methods) that does not result in vibration and magnetic attenuation.

To verify the performance of our shield, we first used a magnetic pickup probe to confirm that at 10 kΩ, the shield does not attenuate the magnetic output of our TMS coil. As Figure 2.3C illustrates, induction

voltage waveforms, with and without the shield, overlap perfectly, confirming the absence of any noticeable magnetic attenuation. Subsequently, using a high-impedance buffer, we measured the voltage between an EEP microelectrode and a ground electrode, both electrode tips immersed in a saline bath, under mspTMS at 100% maximum stimulator output (MSO) delivered with or without the shield. We expected that the shield would remove, to a large extent, voltage signal that is due to electric field coupling between the TMS coil and the EEP recording assembly. Figure 2.3D illustrates the results from these measurements. Without the shield, the captured waveform was drastically different from the induction waveforms resulted by mspTMS, and it ended with a strong voltage bias (polarization; Figure 2.3D left panel). With the shield in place, the captured waveform appeared consistent with the induction waveforms and the voltage bias was no longer visible (Figure 2.3D middle panel). These findings confirm that by interrupting electric field coupling, the shield is effective in preventing polarization and the decay artifact that follows.

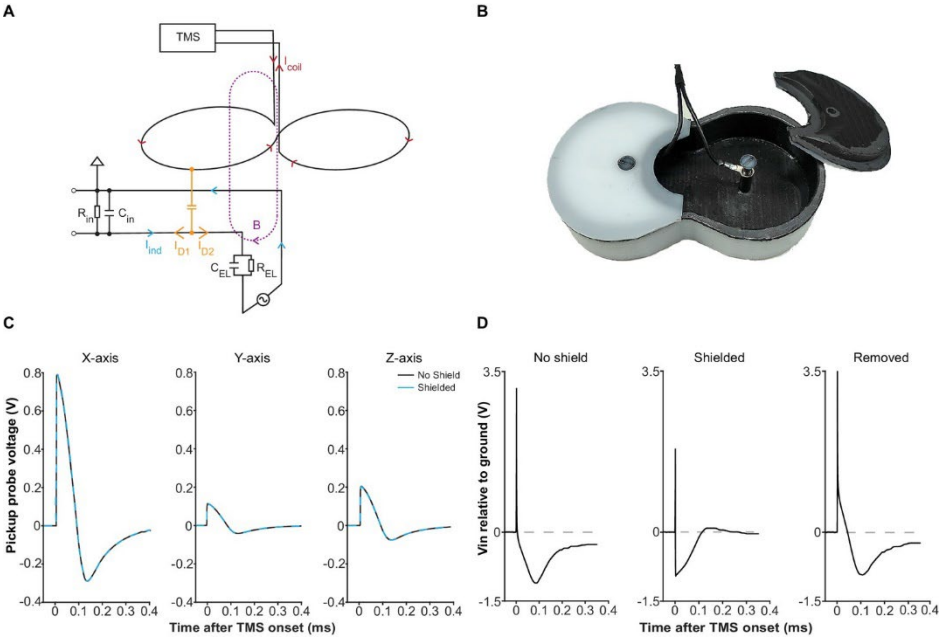

Figure 2.3: Electric field coupling in TMS-EEP and its attenuation. (A) A schematic illustrating how electric field coupling interferes with the EEP recording circuit. Here, the loop between one microelectrode and the ground is used as an example. The microelectrode is modeled as a parallel resistor-capacitor for simplification. Note how displacement current (I_D), generated by electric field coupling, propagates in both directions once it enters the circuit, while the magnetically induced current (I_{ind}) only propagates in a circular manner. The branch of displacement current (I_{D1}) that flows toward the input end of the amplifier opposes the I_{ind}, counteracting the magnetically induced voltage change across the amplifier input resistance (R_{in}). The other branch (I_{D2}) flows toward the electrode and can cause polarization at the microelectrode tip. Abbreviations: *B*, magnetic field; C_{EL}, electrode capacitance; C_{in}, amplifier input capacitance; I_{coil}, TMS coil current; R_{EL}, electrode resistance. **(B)** The electrical shield constructed for the Magstim D25 coil. The shield fits tightly with the coil and is grounded through the EEP recording system. **(C)** Induction waveforms from a pickup probe positioned right below the coil center, along the X-, Y- and Z- axis, with or without the shield, under mspTMS at maximum intensity. Along each axis, the waveforms obtained under shielded and no shield condition overlap, confirming that the shield does not attenuate the magnetic output of the TMS coil. **(D)** Input voltage to a high impedance buffer (AD825, V_s =±15V), measured with a 1.5 MΩ (1 kHz) microelectrode, and an Ag/AgCl ground electrode in normal saline under mspTMS at maximum intensity with or without the shield. Signal in the 'Removed' condition was obtained by taking the difference between the waveforms in 'No shield' and 'Shielded' condition. The shield restored the correct induction waveform and abolished the voltage offset that leads to the decay.

2.2.3 Attenuation of vibration artifacts

Upon elimination of artifacts resulted from induction and electric field coupling, vibration artifacts, which are normally masked by the other artifacts, become visible (Figure 2.4B). Vibration can be generated by magnetic force, as well as by sound pressure perturbation. For the magnetically mediated vibration, an avoidance of ferromagnetic materials and large conductive surfaces in the close vicinity of the coil is adequate. However, the elimination of vibration artifacts driven by sound pressure is not straightforward. When a TMS pulse is triggered, a loud click sound is produced by coil wires due to the attractive forces between them. This sound is problematic as it generates micro-vibration in the amplifier input cables. The extremely weak signal (μV-level) these cables carry can be easily perturbed by micro-vibrations through the triboelectric effect (Fowler, 1976). Since the generation of such click sound is inevitable, we attenuated the vibration artifacts by using a special type of low-noise miniature coaxial cable with a semiconducting layer added between its dielectric and braided shield (Figure 2.4A). The addition of this semiconducting layer provides a path that drains triboelectric charges, rendering the cables insensitive to vibration (Figure 2.4C).

Despite the impressive performance of the low-noise miniature coaxial cable in attenuating vibration artifacts, its length in an EEP recording assembly should be limited as the cable's capacitance (100 pF/m), together with the amplifier input capacitance and electrode impedance, acts as a voltage divider that attenuates EEP signal. In our

case, we kept the length of our cables at 16 cm to keep the signal attenuation less than 20% at 1 kHz.

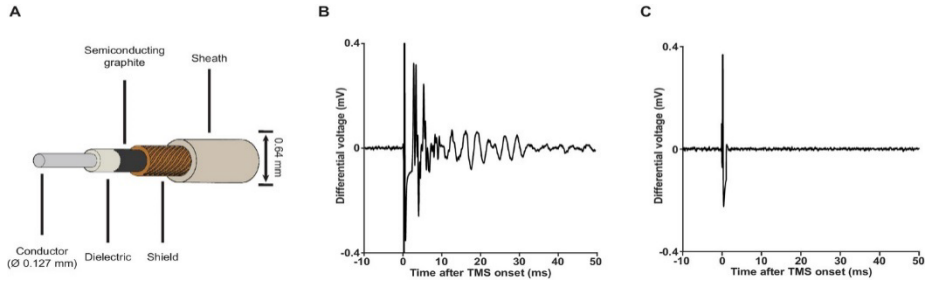

Figure 2.4: Low-noise miniature coaxial cable attenuates vibration artifacts. (A) A schematic illustration of the 36-gauge low-noise miniature coaxial cable. A semiconducting layer of graphite is added between the braided shield and the dielectric of the cable to drain triboelectric charges, rendering the cable insensitive to vibration. **(B)** An example of vibration artifacts recorded under the standard EEP conditions (x2000 using our TMS-EEP amplifier; 1.5 MΩ microelectrode pair; Ag/AgCl ground electrode; normal miniature coaxial cable) in a saline bath after induction and electric field coupling artifacts were suppressed. The vibration artifacts can manifest in multiple types of waveform, depending on the parts of the recording assembly that are perturbed and the resonance properties of these parts. **(C)** The implementation of low-noise miniature coaxial cables attenuated the vibrational artifacts. Signal recorded under conditions identical to those in **(B)** except the cables.

2.2.4 Minimization and determination of inadvertent charge injection

TMS-driven inadvertent charge injection is another major issue, which has been overlooked by most prior reports using EEP under TMS (Moliadze et al., 2003, 2005; Pasley et al., 2009). By inserting electrodes into the brain and connecting them to the measurement electronics, multiple loops of electric circuit are formed (Figure 2.5). When being subjected to alternating electric and magnetic field, voltages can be readily developed along these loops that drive unwanted current injection into the brain through microelectrodes. If the amount and the temporal structure of the injected current are comparable to the

threshold parameters reported in intracortical microstimulation (ICMS) literature (bipolar charge transfer totaling from 150 to 800 pC, current waveform approximately similar to that of TMS; see Asanuma and Rosén, 1973; Butovas and Schwarz, 2003), such current will excite neuronal elements around the microelectrode tips and therefore severely confound the measurement of TMS effects. Therefore, it is crucial that the development of voltages along these loops be minimized. Since a large portion of the TMS-emitted electric field had already been filtered away by the coil shield, precautions were taken for magnetic induction. These included a compact arrangement of microelectrodes as well as cable twisting (Figure 2.5 Supplement 1), both minimize the area of induction loops exposed to TMS. More importantly, we incorporated a low-gain monitoring channel (LGM as seen in Figure 2.2) in our amplifier design that allowed us to conveniently determine the amount of inadvertent current flow, without any additional measurement devices, under each experimental setup. The conversion from voltage, which is measured by the LGM, to current is made possible since amplifier's input capacitance and its voltage fluctuation are known, and the amount of current flow through the input capacitance is equal to the amount of current flow in the circuit. A detailed description of this conversion is presented in Materials and Methods and Figure 2.5 Supplement 2.

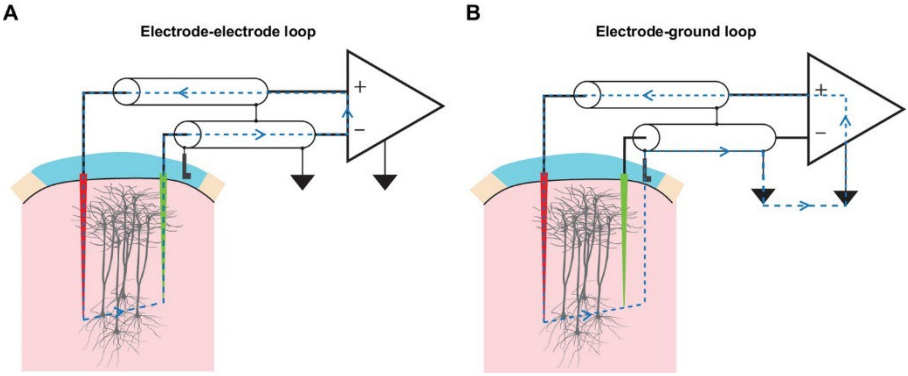

Figure 2.5: TMS drives inadvertent charge injection in multiple loops formed by an EEP recording assembly. (A) A schematic illustration of the induction loop formed between the recording (red) and the reference (green) microelectrode under TMS. In the case that TMS-induced voltage is high enough, a substantial amount of electrical current (blue dashed lines) can flow within the loop and subsequently, this may inadvertently stimulate neuronal elements around the microelectrode tips. **(B)** A schematic illustration of the induction loop formed between a microelectrode and the ground electrode under TMS.

2.2.5 *In vivo* method evaluation under various types of TMS stimuli

In six male Sprague-Dawley rats, we evaluated and optimized our method by conducting concurrent TMS and EEP measurement in the primary forelimb motor area (caudal forelimb area, CFA). Figure 2.6A offers an overview of our recording setup and the subsequent figures illustrate the performance of the method *in vivo* under a single monophasic (Figure 2.6B) and biphasic (Figure 2.6C) TMS pulse, as well as a triplet of 50 Hz biphasic pulses (Figure 2.6D), which is the fundamental building block of theta burst stimulation (Huang et al., 2005). The stimuli delivered here can be considered as the 'worst-case scenarios' as the stimulator-coil combinations used yield magnetic

outputs (peak strength up to four tesla) that are one of the highest among commercially available TMS systems (see Materials and methods). Nonetheless, the EEP signal recovered between 0.8 and 1 ms after the onset of each TMS pulse and was free from artifacts. Furthermore, the amount of inadvertent charge injection under each condition was far below (by a factor of 200 or more; Figure 2.6 Supplement 1) the modulation or activation thresholds reported in ICMS literature (Asanuma and Rosén, 1973; Butovas and Schwarz, 2003), confirming the validity of our measurements.

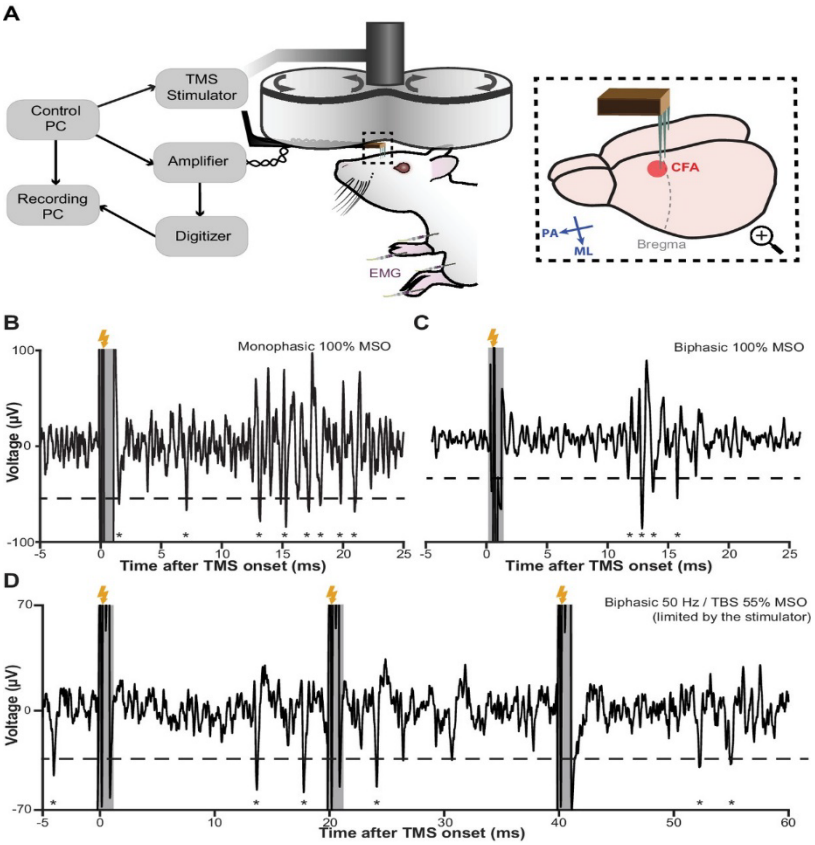

Figure 2.6: TMS-EEP recording setup and rapid signal recovery under the worst-case TMS stimuli. (A) A schematic illustration of our recording setup. Thick arrows, direction of coil current; inset blue arrows, direction of induced current in the brain; ML, medial-lateral; PA, posterior-anterior; CFA, caudal forelimb area (rodent's equivalent to forelimb M1 in primates); EMG, intramuscular electromyography. **(B–D)** A sample trace of in vivo recordings under the worst-possible (see Materials and methods) monophasic, biphasic, and theta-burst (first three pulses) stimulus, respectively. The short transient (−0.2 to +0.8 ms) during which the amplifier is protected from the induction artifact is indicated in gray. Lightning symbol, TMS onset (at 0 ms); dashed line, spike detection threshold (see Materials and methods); asterisks, extracellular spikes.

2.3 Discussion

Our understanding of the neuronal mechanism of TMS has been largely based on indirect evidence obtained at the level of cortical output reflected in spinal cord or muscle activities. Direct investigation of the dynamics of neuronal activities evoked by TMS was hindered by technical obstacles imposed by the strong electromagnetic pulse produced by TMS. We engineered a widely applicable experimental method for the in vivo study of TMS-evoked brain activities at the level of neurons using EEP. It allows the monitoring of neuronal activities as early as 0.8–1 ms after the strong electromagnetic perturbation of various TMS stimuli ranging from single pulse to the high-frequency theta burst stimulation. Our method encompasses solutions to all major challenges in concurrent TMS-EEP recording, including magnetic induction, electric field coupling, vibrations, and inadvertent charge injection. Despite the multidimensional approach of our method, it was developed with generalizability, simplicity, flexibility, and scalability in mind. It is compatible with, but not limited to, rodents, an animal model that is widely used for studying basic neurophysiology and offers a wide range of investigative tools. It does not require active compensation based on magnetic field sensing (Logothetis et al., 2001; Mueller et al., 2014) or custom-made coils (Mueller et al., 2014; Tischler et al., 2011) for artifact reduction. It can accommodate electrodes directly under a conventional TMS coil, a feature making it suitable even for awake animals with chronically implanted electrodes. In addition, the method can be scaled up for large-scale high-density EEP recording with silicon-based microelectrode arrays (Buzsáki, 2004) as well as be accompanied

by optogenetic tools for the in vivo control of neuronal circuits (Scanziani and Häusser, 2009).

The amount of magnetic, electric, and vibrational interference TMS imposed on EEP depends on multiple factors. Some of the most critical factors include the waveform and magnitude of the pulsed magnetic and electric field emitted from a TMS coil, the size of circuit loops formed by an EEP recording assembly, and the coil position relative to these loops. Changes in these parameters will result in changes in the severity of different types of interference. For example, keeping the coil the same, by replacing a standard monophasic with a standard biphasic stimulator, coil-emitted fields will generate a longer period of magnetic and electric field interference due to the longer pulse waveform. However, the severity of interference might be lower if the coil and biphasic stimulator combination does not produce magnetic and electric outputs that are as high as those in the monophasic case. Similarly, miniaturization of TMS coils for small animals can also lead to a reduction in interference because of the reduced electromagnetic output of such devices. Furthermore, the integration of recording, reference, and ground electrode in one microfabricated electrode array can also reduce the severity of interference as such configuration significantly decreases the area of circuit loops exposed to TMS.

One common criticism of TMS investigations in rodents is that the TMS coil is large compared to the size of a rodent brain. While we fully acknowledge this concern, we argue that it is not a problem of critical importance at this stage. With careful coil positioning, it is possible to achieve certain level of spatial selectivity as reported in the

literature (Muller et al., 2014; Nielsen et al., 2007; Rotenberg et al., 2010). In addition, plasticity, assessed by motor output (Muller et al., 2014), learning performance (Mix et al., 2010), sensory-evoked neural activities (Murphy et al., 2016; Thimm and Funke, 2015), or protein expressions (Benali et al., 2011; Trippe et al., 2009), can also be successfully induced in rodents using human TMS coils, making rodents a suitable experimental model for investigating the basic neuronal mechanisms underlying stimulation-induced plasticity. Furthermore, TMS can be used as a tool to deliver a strong transient stimulus to perturb neuronal populations of the neocortex (Walsh and Cowey, 2000). Being able to capture the neuronal response to such perturbation at spike resolution will undoubtedly open another avenue to study the connectivity and the functional properties of neuronal networks. Nonetheless, the development of smaller and more compact coils specifically designed for small animals would be beneficial for their improved spatial resolution and smaller electromagnetic interference as the maximum magnetic output of these coils is much smaller (at mT level; Makowiecki et al., 2014; Tang et al., 2016) than the 4 T output tested in our development.

By combining the tool presented here with optogenetic, transgenic, anatomical, theoretical, and clinical methods, future work studying the neuronal dynamics under TMS will undoubtedly advance our understanding of the functional organization of the brain and drive the development of non-invasive brain stimulation therapies that are more specific, effective, durable and safe than hitherto possible.

2.4 Materials and Methods

2.4.1 Determination of the inadvertent charge injection

To determine the amount of TMS-induced charge injection in the electrode-electrode loop (Figure 2.5A), we used the voltage signal from the low-gain monitoring channel to calculate the current flow via the amplifier's input capacitance C_{in}. As shown in Figure 2.5 Supplement 2, since the input resistance R_{in} and the input capacitance C_{in} are parallel, voltage drop across R_{in} (therefore, the recorded signal V_{in}) is equal to the voltage drop across C_{in}. Because the value of C_{in} is known, its current Ic_{in} can be calculated using the equation

$$I_{Cin} = C_{in}\frac{dV_{in}}{dt}$$

Furthermore, since R_{in} is in the order of teraohm, the amount of current it draws can be neglected. Therefore, Ic_{in} is equal to the total amount of induction current present in the loop (I_{ind}). It is worth noting here that by adopting this method, the exact model of microelectrodes and its associated component values are not needed for the calculation.

For determining the induced charge injection in the electrode-ground loop, we used a set of input cables in which both the recording and the reference electrode were connected to the amplifier's positive input, and the ground electrode was connected to the amplifier's negative input. Furthermore, the negative input was shorted to the amplifier ground. Under this configuration, I_{ind} reflected the current in the electrode-ground loop (Figure 2.5 Supplement 2B).

At the end of our validation, we conducted these measurements in vivo, under monophasic and biphasic TMS, at 100% MSO. By integrating I_{ind} over time, the amount of charge transfer was determined. The results (Figure 2.6 Supplement 1) were then compared with the charge injection values reported in the ICMS literature.

2.4.2 Electrical shield

To construct the electrical shield (Figure 2.3B), we first made a polyoxymethylene (POM) enclosure (1 mm thick at the bottom face) according to the shape of our TMS coil. An even layer of conductive coating (GRAPHIT 33, Kontakt Chemie, Iffezheim, Germany) was painted on the inner side of the enclosure until the desired electrical resistance (10 kΩ measured along the long axes of the shield body and cover) was reached. A layer of non-conductive transparent coating was then applied to protect the conductive layer. As the body and the top covers of the enclosure are separate, protection coating was not applied along the contacting edges between the shield body and its top covers to allow good electrical contact. In addition, an electrical cable was connected directly to the conductive layer to provide a path for grounding.

2.4.3 Animals

All experimental procedures involving animals were approved by the Tübingen Regional Council (license number: N1/16) and performed in accordance with the Animal Welfare Act of Germany. Six male Sprague-Dawley rats (Charles River Laboratories, Sulzfeld, Germany) 11–15 weeks of age were used. The animals were housed in

environment-enriched transparent plastic cages under inverted 12 hr light/dark cycle with free access to water and food. Upon arrival, the animals were handled 10 min per day for 5 consecutive days for stress reduction.

2.4.4 Surgery

Animals were first sedated through a brief exposure to isoflurane (3% at 0.8 L/min). Upon sedation, a cocktail of ketamine (70 mg/kg) and xylazine (1 mg/kg) was injected intraperitoneally (i.p.) and ophthalmic ointment was applied to eyes. A 27-gauge catheter was implanted in the lower right quadrant of the abdomen to provide i.p. access throughout the experiment. Additional doses of ketamine (30 mg/kg) were administered through the catheter to maintain a constant level of anesthesia, which was assessed by breathing rate, vibrissa whisking, and the toe-pinch reflex. During the incision phase of the surgery, xylocaine gel (2%) was applied to the incision site. In addition, body temperature of the animals was maintained at 37°C using a feedback-controlled heating pad throughout the experiment.

Animals were restrained in a stereotaxic frame with non-conductive ear bars. A 5 × 3 mm craniotomy was made over the left sensorimotor cortex. The resulted trepanation extended from −1 mm to +4 mm to bregma and from 1 mm to 4 mm lateral to the midline. Dura matter was carefully resected and the cranial window was covered with Ringer's solution.

2.4.5 Transcranial magnetic stimulation (TMS)

TMS was delivered through a Magstim D25 figure-of-eight coil (single circle radius 25 mm; Magstim Ltd., Carmarthenshire, UK) powered by either a Magstim 200^2 stimulator for monophasic single-pulse stimulation (mspTMS) or a Magstim Super Rapid Plus stimulator (with the inline inductor Magstim 3467) for biphasic single-pulse and repetitive stimulation. The Magstim 200^2 and D25 combination is considered as the worst-case scenario since the resulting flux transient is as high as 4T (based on data supplied by Magstim), which is two to three times higher than the output seen in combinations with larger coils that are routinely used in human stimulation.

The TMS coil was held by a mechanical arm and positioned over the recording site in medial-lateral orientation, generating a current flowing from the medial to the lateral part of the brain (under monophasic stimulation). In the PA orientation, the induced current flows from the posterior to the anterior part of the brain. The coil, controlled by a three-dimensional microdrive, was lowered as much as possible without touching the electrode assembly. The distance from the coil surface to the head of the animal was normally 8–10 mm (including 1 mm due to the coil shield). TMS was triggered digitally by a controller PC, which also digitally controlled the behavior of our EEP amplifier (Figure 2.6A).

2.4.6 Extracellular electrophysiology (EEP)

EEP was recorded through a pair (signal-reference) of microelectrodes (ca. 1.5 MΩ impedance at 1 kHz) fabricated in-house from glass-coated platinum-tungsten wires (Thomas RECORDING,

Giessen, Germany). A thin silver wire with silver-chloride coating was used as the ground electrode. The three electrodes were arranged in a three-pronged design (Figure 2.5 Supplement 1) that minimized the induction loop area between them. The assembly was held by a non-conductive non-magnetic L-shape holder that was mounted on a micropositioner (David Kopf Instruments, Tujunga, USA). The recording electrode was lowered, through the cranial window, into CFA as determined by ICMS. The reference electrode was also lowered into the cortex but outside the boundary of CFA. The ground electrode was positioned to be in contact with unresected subcutaneous tissue by the border of the cranial window. Signals from the electrodes were transmitted through a pair of twisted 36-gauge low-noise miniature coaxial cables (Axon' Cable S.A.S., Montmirail, France; Figure 2.4A) to the amplifier. The operating mode of the amplifier was controlled by the controller PC as described in the main text. The signal from the amplifier output was digitized (USB-ME64-System, MultiChannel Systems GmbH, Reutlingen, Germany) at 40 kHz and subsequently visualized and stored on a PC. A schematic illustration of the entire recording setup is shown in Figure 2.6A.

2.5 Contributions

Bingshuo Li: conceptualization, data curation, data analysis, writing – original draft, writing – review and editing;

Alia Benali: conceptualization, data curation, data analysis, writing – original draft, writing – review and editing, daily supervision;

Juha Virtanen: methodological development, writing – review and editing;

Axel Oeltermann: methodological development, writing – review and editing;

Cornelius Schwarz: laboratory resources, funding, data interpretation, writing – review and editing, supervision;

Martin Giese: laboratory resources, funding, data interpretation, writing – review and editing, supervision;

Ulf Ziemann: laboratory resources, funding, data interpretation, writing – review and editing, supervision.

2.6 Acknowledgements

We express our gratitude to Oliver Holder (Max Planck Institute for Biological Cybernetics), Eduard Krampe (Max Planck Institute for Biological Cybernetics), Ursula Pascht (Uni. Tübingen), Klaus Vollmer and associates (Uni. Tübingen) for technical support; Klaus Funke (Uni. Bochum) for equipment loan and comments; Nikos Logothetis (Max Planck Institute for Biological Cybernetics) for logistical support and comments; Florian Müller-Dahlhaus (Uni. Tübingen), and Dominic Kraus (Uni. Tübingen) for comments.

2.7 Supplementary Information

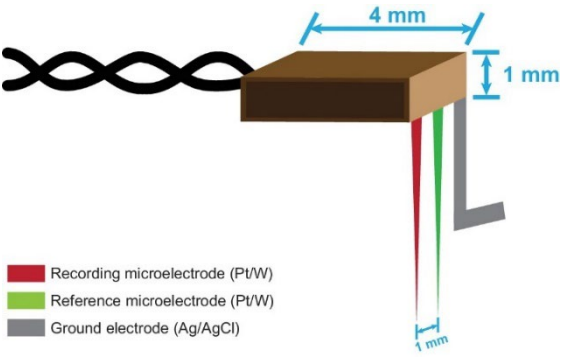

Figure 2.5 Supplement 1: The three-pronged electrode set design. We fabricated in-house a three-pronged electrode set that minimizes the area of induction loops under TMS. The microelectrodes are connected to a pair of twisted low-noise miniature coaxial cables, and the ground electrode is connected to the coaxial cable shield. A macroscopic view of the electrode set in a recording setup is shown in Figure 2.6A.

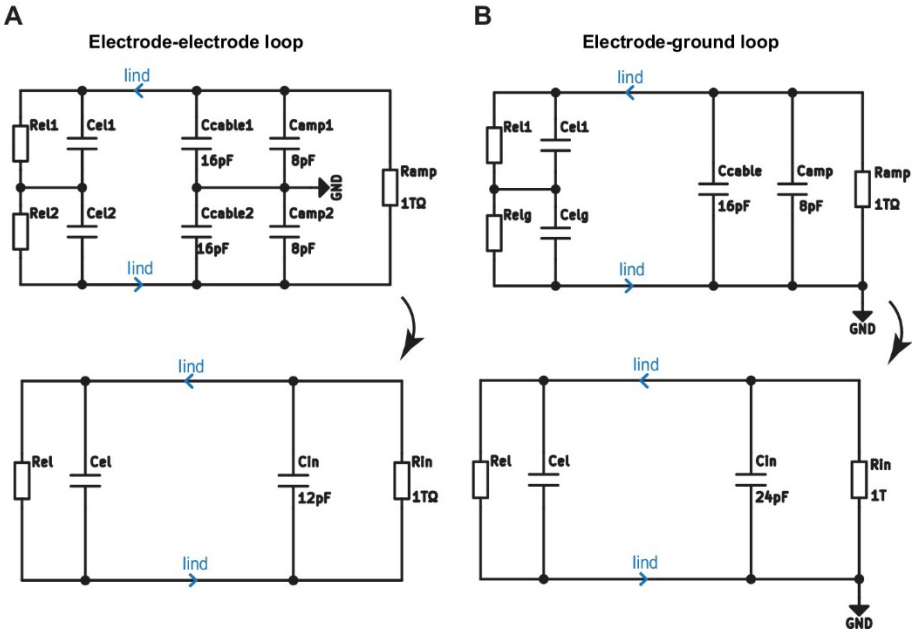

Figure 2.5 Supplement 2: Circuit representations of the two induction loops shown in Figure 2.5. Circuit component abbreviations: *amp*, amplifier; *C*, capacitance; *el1*, recording microelectrode; *el2*, reference microelectrode; *elg*, ground electrode; *GND*, amplifier ground; *in*, input; *Iind*, induction current; *R*, resistance.

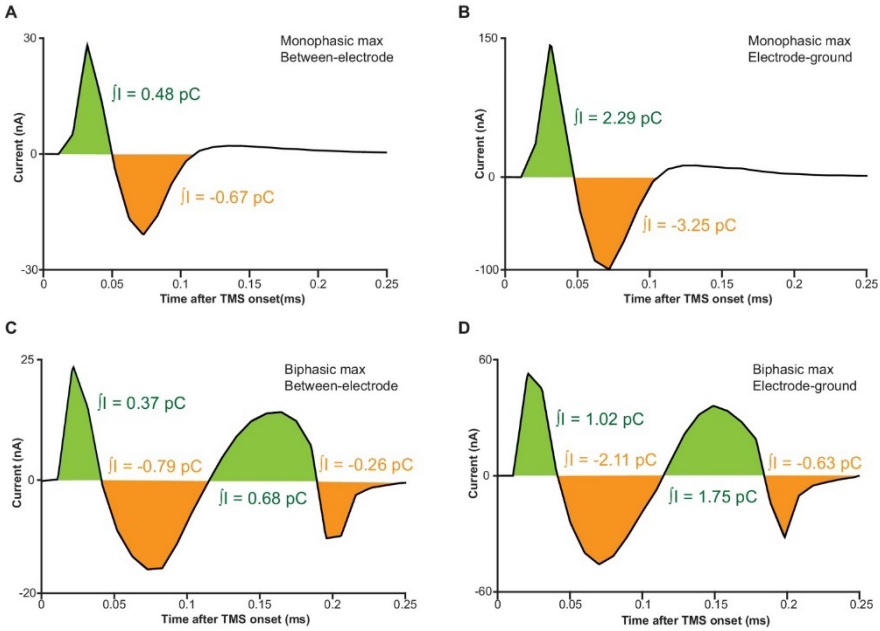

Figure 2.6 Supplement 1: *In vivo* measurements of inadvertent charge injection. Under the worst-possible stimuli (see Materials and methods), the in vivo measured values of induction current (y-axis) and charge transfer (integral of y) are shown. All values obtained are far below (by a factor of 200 or more) the modulation and the activation thresholds reported in the ICMS literature (Asanuma and Rosén, 1973; Butovas and Schwarz, 2003). Therefore, it can be concluded that under our recording setup, neurobiological effects of inadvertent charge injection can be neglected.

3. Characterizing the dynamics of neuronal activities in M1 evoked by a monophasic single-pulse TMS

This chapter is adapted from the following publication:

Li, B., Virtanen, J.P., Oeltermann, A., Schwarz, C., Giese, M.A., Ziemann, U., and Benali, A. (2017). Lifting the veil on the dynamics of neuronal activities evoked by transcranial magnetic stimulation. *eLife*, 6, 1–22.

3.1 Introduction

Upon the successful development of a methodological advance for concurrent TMS and EEP, we are at the position to uncover TMS-evoked neuronal activities in M1 when the TMS stimulus behaviorally evokes contractions of selected limb muscles, as demonstrated by Barker et al. (1985). To this end, in anesthetized rats, we delivered mspTMS to caudal forelimb area (CFA), rodent's equivalent to the forelimb area of primate M1, to evoke unilateral forelimb muscle contractions. Concurrently, we recorded extracellular neuronal activity in the output layer (layer V) of CFA using EEP and motor unit action potential (MUAP) in the biceps brachii muscle using intramuscular EMG.

3.2 Results

3.2.1 mspTMS-evoked unilateral biceps brachii activation is of cortical origin

With the center of the TMS coil positioned over the left CFA and the induced current pointing from the medial to the lateral part of the brain (ML stimulation; Figure 2.6A inset), mspTMS evoked unilateral movement of the right forelimb. Simultaneous intramuscular EMG recordings of the left and right biceps brachii muscle revealed MUAPs unilaterally in right biceps brachii (contralateral to the stimulated hemisphere; Figure 3.1B and the insets of Figure 3.1C–F). The onset latency of the MUAPs was around 11 ms, similar to that found in a control experiment in which we delivered single-pulse ICMS to the layer V of CFA (Figure 3.1 Supplement 1) and to the results reported in rodent

ICMS literature (Deffeyes et al., 2015; Liang et al., 1993), thereby confirming the cortical origin of TMS-evoked muscle activation.

3.2.2 mspTMS evokes in the layer V of CFA a multiphasic rhythm of neuronal activities

At the neuronal level, in layer V of the CFA (Figure 3.1 Supplement 2), mspTMS evoked a rhythm of neuronal activities alternating between excitation and inhibition that lasted until approximately 300 ms post-stimulation. Figure 3.1A illustrates the multiunit spike raster and its corresponding peristimulus time histogram (PSTH) of multiunit firing rate (FR) from one animal. Figure 3.1C–F show the evoked normalized FR (instantaneous FR subtracted by baseline average FR; see Materials and Methods) with increasing stimulation intensity (0%, 95%, 100%, and 120% motor threshold, MT) averaged across all animals (N = 7). Significance thresholds were drawn based on the 2.5 and 97.5 percentile of the empirical distribution of normalized FR during baseline (500 ms pre-TMS; see Materials and Methods) to control Type I error rate ($p<0.05$). We categorized the evoked significant excitatory and inhibitory events into three phases: intermediate excitation (a period of increased FR that peaks around 20 ms), inhibition (a long-lasting pause in FR after the intermediate excitation), and rebound excitation (a period of increased FR following the inhibition). To investigate the effects of stimulation intensity on the normalized FR of each phase, we constructed hierarchical linear mixed-effects models. Stimulation intensity positively modulated the normalized FR for the intermediate excitation phase ($\beta = 2.75 \pm 0.24$, $F(1)=127.23$, $p<0.001$)

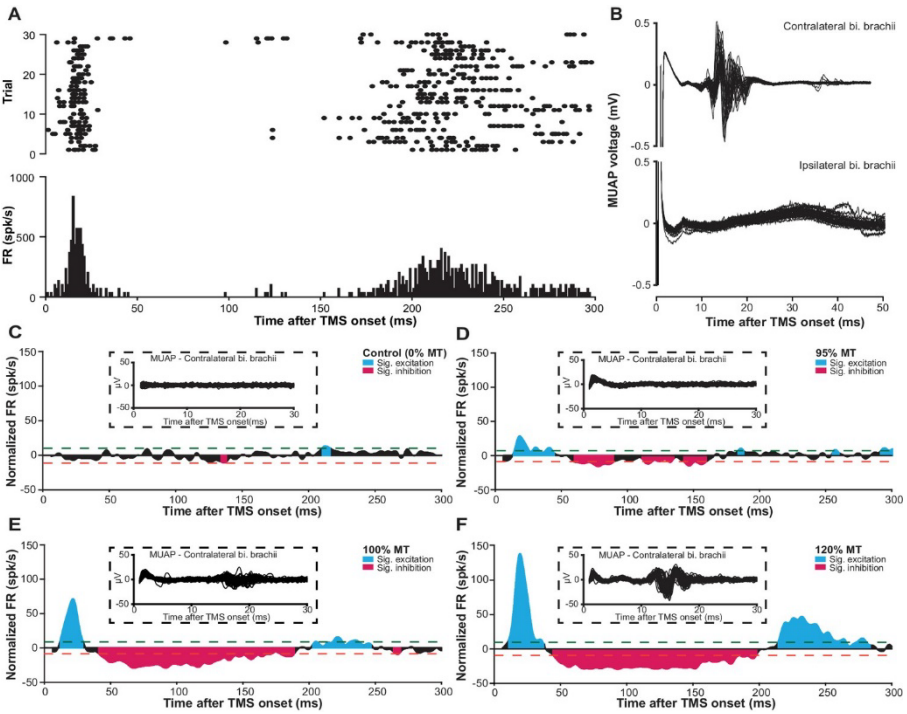

Figure 3.1: mspTMS evoked multiphasic response alternating between excitation and inhibition. (A) Raster plot (top) and PSTH (bottom; binsize 1 ms) of multiunit spike activity evoked by mspTMS (stimulus orientation ML; intensity 120% MT; onset at 0 ms) recorded in layer V of the CFA from one animal. **(B)** Traces of evoked MUAPs (corresponding to trials in A) obtained by intramuscular EMG in the biceps (bi.) brachii muscle contralateral and ipsilateral to the stimulated CFA. **(C–F)** Population average (N = 7) of normalized multiunit FR in the layer V of CFA evoked by ML-oriented mspTMS of increasing intensity. The PSTHs were smoothed by a Gaussian kernel for visualization. Inset, example traces of evoked MUAP in the contralateral bi. brachii from one animal. Dashed lines, significance thresholds determined by the 2.5 or 97.5 percentile of the empirical distribution of baseline normalized FR (see Materials and methods for details).

and the rebound excitation phase ($\beta = 1.18 \pm 0.19$, $F(1)=38.65$, $p<0.001$), while negatively modulated the normalized FR for the inhibition phase ($\beta = -0.23 \pm 0.10$, $F(1)=5.28$, $p=0.02$). It is important to

note here that despite the faithful EMG response in the contralateral biceps brachii muscle, the neuronal firing rate in the short-latency window (1-6 ms after TMS onset) was low. This finding was rather surprising and will be further explored in the following section.

3.2.3 mspTMS evoked short-latency (1-6 ms) neuronal responses differ with stimulus orientations

Since we did not observe any significant modulation of neuronal FR in the short-latency window (1-6 ms) after mspTMS despite faithful muscle activations in the contralateral forelimb, in another set of experiments (N = 4), we explored the possibility that neuronal response in this very early time window is dependent on the direction of mspTMS-induced current. In this set of experiments, we switched the TMS coil orientation so that the induced current flows from the posterior to the anterior part of the brain (PA stimulation; Figure 2.6A inset). We could replicate most findings found in the previous set of experiments as the multiphasic response evoked by PA stimulation is qualitatively similar to that evoked by ML stimulation (Figure 3.2). However, in the short-latency window after TMS onset, the neuronal responses observed in ML and PA stimulation are drastically different. As the two examples in Figure 3.2A demonstrate, at 120% MT intensity, ML stimulation evoked scarcely any spike, whereas PA stimulation evoked robust neuronal firing generating a distinct temporal pattern with peaks at 1.2-1.6 ms and at 3.2-4.2 ms. To quantify the short-latency responses in the population, we constructed PSTHs of normalized FR across all animals under ML (Figure 3.2B) and PA (Figure 3.2C) stimulation. Significance thresholds

were drawn using the 2.5 and 97.5 percentile of normalized FR distribution during baseline. ML stimulation evoked no significant excitation with the exception of the low albeit significant FR at 3.5-4 ms under stimulation intensity of 120% MT. On the contrary, under PA stimulation, multiple significant excitatory events were observed. At subthreshold level, significant excitatory events appeared at 2.5-3.5 ms and at 4-4.5 ms. As stimulation intensity increased, FR was developed at particular time windows: 1-1.5 ms and 2.5-4.5 ms, reminiscent of the

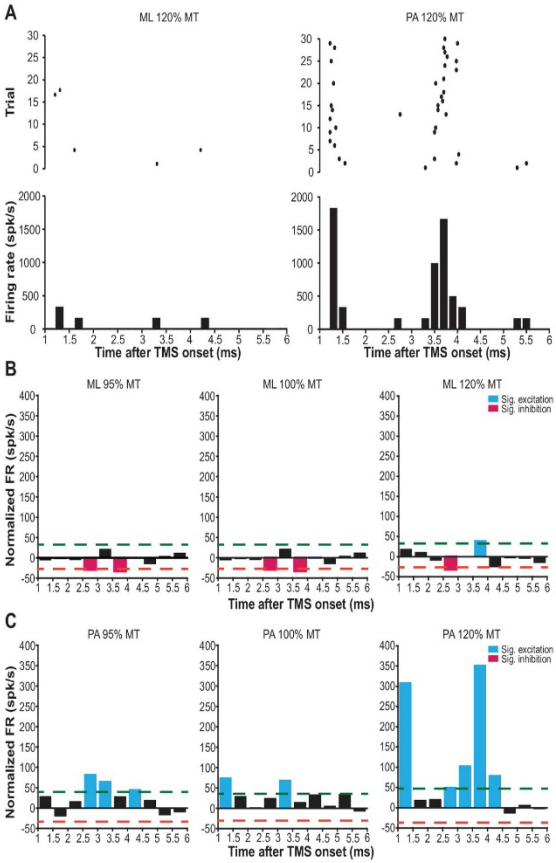

Figure 3.2: mspTMS-evoked short-latency neuronal responses differ with stimulus orientations. (A) Examples of short-latency (1–6 ms) multiunit response in layer V of the CFA to suprathreshold mspTMS (120% MT) oriented in ML and PA direction. The suprathreshold ML stimulus evoked virtually no response in this time window, whereas the PA stimulus evoked strong periodic firing in the neuronal population. Note, all orientations discussed here refer to the orientation of induced current in the brain. **(B–C)** Average of short-latency normalized multiunit FR (binsize 0.5 ms) across all animals tested with the ML- (B) and PA- (C) oriented mspTMS at increasing intensities. Dashed lines, significance thresholds determined by the 2.5 or 97.5 percentile of the empirical distribution of baseline normalized multiunit FR (see Materials and methods for details).

I-wave phenomena observed in the corticospinal descending volleys in human and animal studies.

3.3 Discussion

We successfully translated mspTMS to rodents and captured the evoked neuronal activities underlying this classical TMS stimulus which has been widely used in humans since its introduction in 1985 (Barker et al., 1985). At the behavioral level, mspTMS delivered in either ML or PA direction over left CFA evoked unilateral forelimb movement in the contralateral side. The similarity between the onset latency of mspTMS- and single-pulse ICMS-evoked MUAPs suggests the cortical origin of the TMS-evoked muscle activations. At the neuronal level, despite the similar evoked motor outputs, mspTMS delivered in the ML and PA orientation evoked different CFA layer V neuronal activities in the short-latency window (1-6 ms) after TMS onset. While threshold or suprathreshold ML oriented stimuli evoked virtually no response in this time window, PA oriented stimuli evoked population spiking activities that occurred preferably around 1-1.5 ms and at 3-3.5 ms (Figure 3.2). Such discrepancy in neuronal response suggests that TMS-induced current of different orientations activates different microcircuits in the rodent forelimb M1: ML-oriented stimuli directly activated pyramidal cells of the descending motor pathways while PA-oriented stimuli evoked trans-synaptic high-frequency spiking activities in M1 (Figure 3.3A). It is important to note here that neuronal activity within 1 ms after TMS onset is not visible. Therefore, any antidromic spike evoked by direct axonal activations could not be recorded.

It might be argued that the observed discrepancy in short-latency response is a result of bias in neuronal sampling. We believe this is rather unlikely, as short-latency spikes evoked by ML stimulation were absent across multiple recording sites within CFA (0 out of 7 sites) while the significant high-frequency spiking pattern was observed readily within CFA under PA stimulation (3 out of 4 sites). Additionally, the observed high-frequency spiking as seen in PA trials disappeared when, in the same experiment/animal, we turned the stimulus orientation to ML. While we cannot rule out the possibility that mspTMS evoked early spike responses in areas other than the ones we monitored, our data supports the notion that in the layer V of CFA, the output layer of the rodent forelimb M1, selectivity in stimulus orientation exists. Another confounding factor that might explain the discrepancy is the intensity difference of induced electric fields in the brain under ML and PA stimulation. Since the rodent skull is not spherical, with a given coil output, induced electric field in the ML direction (along the short axis of the skull) should be lower in intensity than that in the PA direction (along the long axis of the skull), raising the possibility that the observed high-frequency spiking pattern under PA stimulation is a result of high intensity of the induced electric field. However, motor thresholds under ML stimulation, in which induced electric field intensity is lower, were significantly lower than their PA counterparts ($median_{ML}$ = 61% MSO; $median_{PA}$ = 74% MSO; Wilcoxon rank-sum test, p=0.03). This is a strong indication that factors other than induced electric field intensity play a critical role in stimulus orientation selectivity. Therefore, we conclude that the observed response difference between ML and PA stimulation

is unlikely to be caused solely by the difference in the intensity of induced electric fields.

TMS studies on human (Kaneko et al., 1996; Di Lazzaro et al., 2001) and non-human primates (Amassian and Stewart, 2003; Amassian et al., 1990) also reported similar stimulus orientation selectivity but in the context of evoked motor outputs. However, we stress that the similarities between our results and those of humans and non-human primates rest solely at the level of a shared common principle: TMS-evoked direct activation is a product of the interaction between TMS-induced electric field and the anatomical and physiological properties of the neurons within. Despite different levels of complexity between primate and rodent brains, certain neuronal structures are preferably stimulated in one stimulus orientation rather than the others. But whether such similarity is based on shared anatomical and physiological properties warrants further investigation. Furthermore, the primate cortex is gyrencephalic while the rodent cortex is lissencephalic. As we could reliably stimulate a lissencephalic M1 and evoke muscle activation on the contralateral forelimb at the correct cortically evoked latency, the locus of direct TMS activation is most likely not dependent on the magnitude of induced electric field component normal to the cortical columns (Bungert et al., 2016; Fox et al., 2004).

The evoked short-latency response in the PA orientation was characterized by population spikes at a very high frequency similar to that of the I-waves recorded in the corticospinal tracts of humans and animals in response to a transient shock delivered to the M1 by either transcranial electrical stimulation (Kernell and Chien-Ping, 1967; Patton

and Amassian, 1954) or TMS (Kaneko et al., 1996; Di Lazzaro et al., 2012; Nakamura et al., 1996). What are the principles of anatomical and functional organization in M1 that drive such high-frequency neuronal response? We recorded in layer V of the motor cortex (Figure 3.1 Supplement 2) where two types of excitatory projection neurons exist: the pyramidal tract (PT) neurons that project to midbrain, brainstem, and spinal cord, and the intratelencephalic (IT) neurons that project ipsi- or bilaterally within the cortex and striatum (Harris and Shepherd, 2015). It has been shown recently that PT neurons exhibit reciprocal connectivity characterized by short-term facilitation and that synaptic transmission time for a pair of reciprocally connected PT neurons is 1.6 ± 0.5 ms (Morishima and Kawaguchi, 2006; Morishima et al., 2011). Therefore, it is plausible that the network formed by the interconnected PT neurons in layer V provides the physiological foundation for the high-frequency neuronal discharge and that an mspTMS pulse oriented in PA direction preferably delivers an input into this network that triggers the observed high-frequency spiking response (Figure 3.2; Figure 3.3A). Furthermore, the interconnected PT network may also offer a neuronal explanation for the short-interval intracortical facilitation (SICF) described in the human literature (Tokimura et al., 1996; Ziemann et al., 1998).

As we extend the window of investigation to 6-300 ms after TMS onset, a multiphasic response appears among the recorded CFA layer V neurons. The response is characterized by its excitation-inhibition-excitation pattern and is not qualitatively different between PA and ML stimulations (Figure 3.1). The strong excitation that peaks around 20 ms, given its latency, duration, presence in both layer V and II/III (Figure 3.1

Supplement 3), and its apparent lack of motor output (Figure 3.1B), reflects a high excitability state of the motor cortex. We hypothesize that this excitation is generated through the cortico-basal ganglia-thalamo-cortical loops (Figure 3.3B). Evidence suggests that cortex projects monosynaptically to basal ganglia (BG) structures such as striatum and subthalamic nucleus (STN) (Kita and Kita, 2012), while the projection from striatum and STN back to cortex is polysynaptic (Shepherd, 2013). Deep brain stimulation (DBS) of the STN produces cortically evoked EEG potentials with a peak latency of 22.2 ± 1.2 ms, and TMS delivered at this latency after DBS showed facilitation of its cortically evoked motor outputs (Kuriakose et al., 2010). It is likely that TMS activates IT and PT neurons, which in turn project to BG monosynaptically, and the response is then transmitted back to the cortex as the intermediate excitation observed here. But other cortico-cortical or cortico-subcortical loops could be involved as well. The neuronal mechanism of TMS protocols such as intracortical facilitation (Ziemann et al., 1996) and theta burst stimulation (interpulse interval of 20 ms within each burst) (Benali et al., 2011; Suppa et al., 2016) remain unknown; however, it is conceivable that these protocols exploit this particular phase of excitation for their physiological effects. The long-lasting inhibition phase that follows the intermediate excitation is well-known, and evidence supports the notion that it is mediated by $GABA_B$ (Butovas et al., 2006; Murphy et al., 2016) and underlies the long-interval intracortical inhibition as well as the cortical silent period in human TMS (McDonnell et al., 2006; Valls-Solé et al., 1992). However, the local or long-distance circuit mediating this phase of inhibition remains unknown. The rebound excitation phase,

occurring after the inhibition, represents a period of excitation most likely resulting from the termination of $GABA_B$ inhibition, and corresponds to the late cortical disinhibition, which is being harnessed for augmenting plasticity induction in human TMS (Cash et al., 2016). Similarly, the circuit mechanism behind this phase of rebound excitation remains to be elucidated as well.

Would the same neuronal activity pattern be observed if a rodent-sized TMS coil is used to stimulate the forelimb M1? We believe that this is the case since we carefully calibrated coil position and stimulation strength according to MEP. Furthermore, the long-lasting inhibition and the rebound excitation are well-documented phenomena in ICMS (Butovas and Schwarz, 2003), which is a much more localized stimulation method than TMS. Additionally, as discussed above, data from human TMS is largely congruent with the pattern of neuronal activity reported here. However, we cannot rule out the possibility that the coil we used in this study directly activated structures outside of the forelimb M1. Nonetheless, the role of stimulus spatial resolution in modulating neuronal networks is a highly interesting topic for future research.

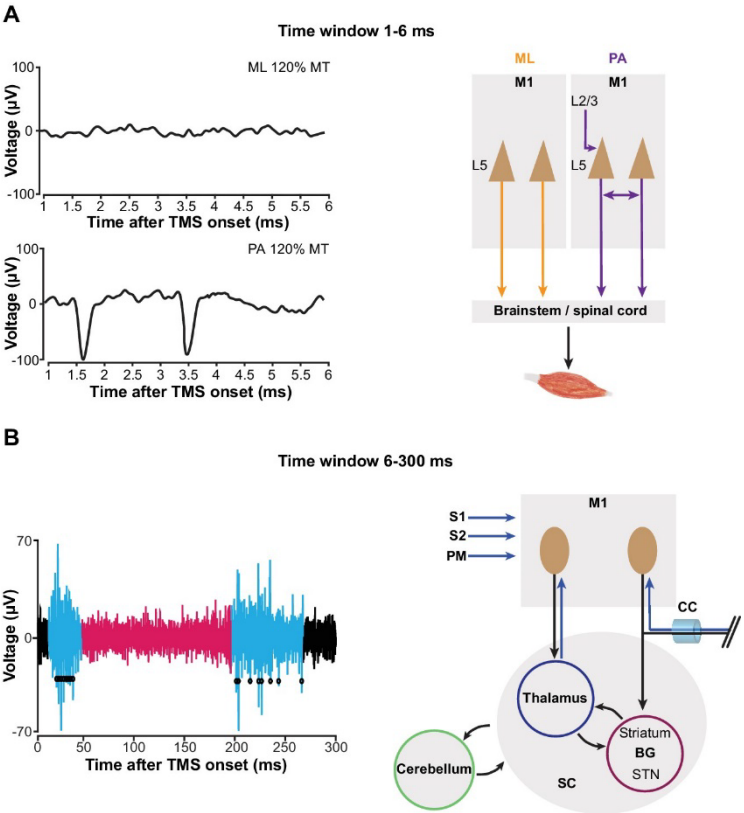

Figure 3.3: mspTMS activates different neuronal circuits depending on stimulus orientation or the time-window of investigation. (A) In the short-latency time window (1–6 ms after onset), ML- and PA-oriented mspTMS evoked different patterns of neuronal activities in layer V of CFA (left panel). ML stimuli activated the descending PT pathways, while PA stimuli triggered an oscillatory spiking event that reflects the local connectivity within M1 (right panel). **(B)** In the long-latency time window (6–300 ms after onset), mspTMS evoked a multiphasic response alternating between excitation and inhibition (left panel shows a raw spike trace evoked by a suprathreshold stimulus; blue and red code for phase of significant excitation and inhibition, respectively, adopted from Figure 3.1). This multiphasic pattern is generated through multiple possible long-range circuits activated by mspTMS (right panel). Abbreviations: *BG*, basal ganglia; *CC*, corpus callosum; *M1*, primary motor cortex; *PM*, premotor cortex; S1/S2, somatosensory cortices; *SC*, subcortical structures; *STN*, subthalamic nucleus.

3.4 Materials and Methods

3.4.1 Animals

Identical to 2.2.3 except animal N = 11.

3.4.2 Surgery

Identical to 2.4.4.

3.4.3 Transcranial magnetic stimulation (TMS)

Identical to 2.4.5.

3.4.4 Extracellular electrophysiology (EEP)

Identical to 2.4.6.

3.4.5 Intracortical microstimulation (ICMS)

ICMS was used to map the spatial extent of the CFA. A platinum-tungsten microelectrode (1 MΩ at 1 k Hz) was used for ICMS at depths around 1400 μm (from the cortical surface), corresponding to layer V in rat neocortex, with a train of 13 biphasic square pulses (200 μs per phase) delivered at 333 Hz using a waveform generator (STG1002, MultiChannel Systems, Reutlingen, Germany). A stimulation site was considered non-responsive if it was not possible to elicit any visible movement with current intensity up to 100 μA.

3.4.6 Electromyogram (EMG)

28-gauge monopolar EMG electrodes (Ambu A/S, Ballerup, Denmark) were implanted in both left and right biceps brachii muscle for recording, and in the finger pads bilaterally for reference. The electrodes were connected to a high-impedance amplifier through shielded cables. The signal was low-pass (cutoff frequency 5 kHz) filtered online and amplified 2000 times before digital conversion. During analysis, the signal was bandpass filtered (100–1000 Hz) using digital Butterworth filters implemented anti-causally.

3.4.7 Histology

Upon completion of an experiment, the recording site was marked by an electrolytic lesion (1 cycle of cathode leading 0.1 Hz biphasic square pulse with 10 μA) generated using a microelectrode powered by a waveform generator (STG1002, MultiChannel Systems, Reutlingen, Germany). Subsequently, the animal was deeply anesthetized with sodium pentobarbital (200 mg/kg) and perfused using phosphate buffer (0.1 M) followed by paraformaldehyde (4%). Afterward, the brain of the animal was processed using standard histological procedures. The recording layer was assessed by investigating lesions in hematoxylin and eosin stained coronal sections.

3.4.8 Quantification and statistical analysis

Electrophysiological data was processed in MATLAB 2014b (The Mathworks, Natick, USA). Spike detection was based on amplitude threshold that was set to 3.5 or 4 times of the median-based background

noise standard deviation estimate in order to minimize the influence of high spike rates or amplitudes in biasing spike detection (Quiroga et al., 2004). Spike isolation was performed using principal component analysis of the spike waveforms followed by a Gaussian mixture model with Kalman filters that track waveform drifts over time (Ecker et al., 2014). A total of 51 single units were isolated ($L5_{ML}$ = 19; $L5_{PA}$ = 14; $L2/3_{ML}$=18); however, since at the present stage we are only interested in characterizing the response of M1 neuronal population to mspTMS, in the following analysis, we combine spikes from all single units as well as those that cannot be reliably isolated into a multiunit cluster.

Each trial was defined by the time interval spanning from 500 ms pre-TMS to 1000 ms post-TMS. Normalized FR was calculated by subtracting the baseline (500 ms period prior to TMS onset) average FR from the instantaneous FR of each time bin (including baseline bins). This normalization procedure was performed on a trial-by-trial basis. For each animal under each stimulation condition, trains of normalized FR were averaged across trials. Thresholds for significant ($p<0.05$) inhibitory and excitatory events were determined by the 2.5 and 97.5 percentile of the empirical distribution of normalized FR during baseline. To facilitate the detection of significant phasic response, each averaged train of normalized FR was filtered by a Gaussian kernel (σ = 2 ms). An event is considered as a significant phasic response if the normalized FR exceeds either threshold for more than 10 ms and a gap up to 10 ms is tolerated to accommodate jittering. The onset and duration information of the detected phasic response was then used to extract FR for each phase in each individual trial.

Statistical analysis was performed in R (R Core Team, 2016). Multiple hierarchical linear mixed-effects models were constructed using the lme4 package (Bates et al., 2015) to evaluate the effect of stimulation intensity on the normalized FR for each response phase. Stimulation intensity (normalized to %MT) was used as the fixed effect to model trials of normalized FR of each response phase. The animal's identity was used as the random effect (random intercept) to control for intraclass correlation. We also explored the possibility of trial number being another fixed effect. However, it was dropped in the final models as it did not contribute significantly to model's fit. Statistical significance of the fixed effect in each model was evaluated against the corresponding null model using the Kenward Roger-based F-test (Halekoh and Hoejsgaard, 2014).

3.5 Contributions

Bingshuo Li: conceptualization, data curation, data analysis, writing – original draft, writing – review and editing;

Alia Benali: conceptualization, data curation, data analysis, writing – original draft, writing – review and editing, daily supervision;

Juha Virtanen: methodological development, writing – review and editing;

Axel Oeltermann: methodological development, writing – review and editing;

Cornelius Schwarz: laboratory resources, funding, data interpretation, writing – review and editing, supervision;

Martin Giese: laboratory resources, funding, data interpretation, writing – review and editing, supervision;

Ulf Ziemann: laboratory resources, funding, data interpretation, writing – review and editing, supervision.

3.6 Supplementary Information

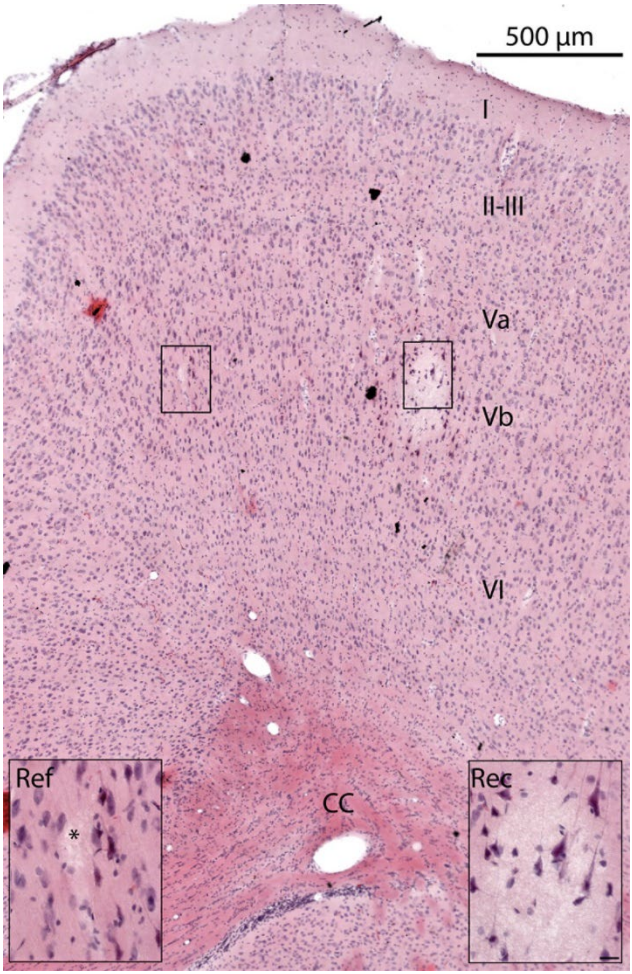

Figure 3.1 Supplement 1: Histological confirmation of electrode placement. The hematoxylin and eosin-stained coronal section confirms the placement of recording electrode (Rec) in layer Vb of CFA and the placement of reference electrode (Ref) outside of the primary motor cortex. The location of Rec was marked by an electrolytic lesion after the experiment and the location of Ref, while not marked by lesioning, is also visible (* in the left inset). The scale bar for the insets represents 20 µm distance. CC indicates corpus callosum. Latin numbers I to VI represent the different cortical layers.

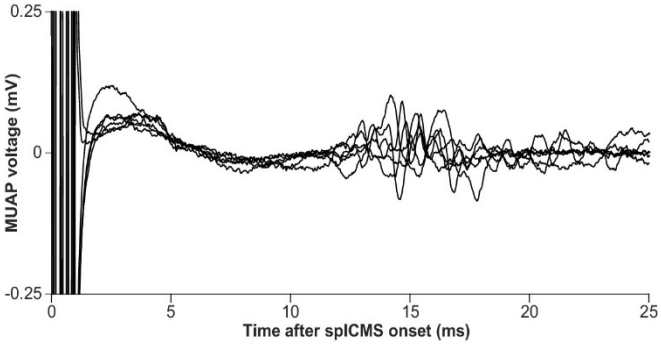

Figure 3.1 Supplement 2: MUAP evoked by single-pulse ICMS. In one animal, we stimulated layer V of the left CFA with a single ICMS pulse and recorded intramuscular EMG in both left (ipsilateral to the stimulated motor cortex; not shown) and right (contralateral) biceps brachii. The evoked MUAPs, detected solely in the right biceps brachii, displayed onset latencies (11–12 ms) similar to those obtained in our TMS experiment, suggesting the cortical origin of the TMS-evoked MUAPs.

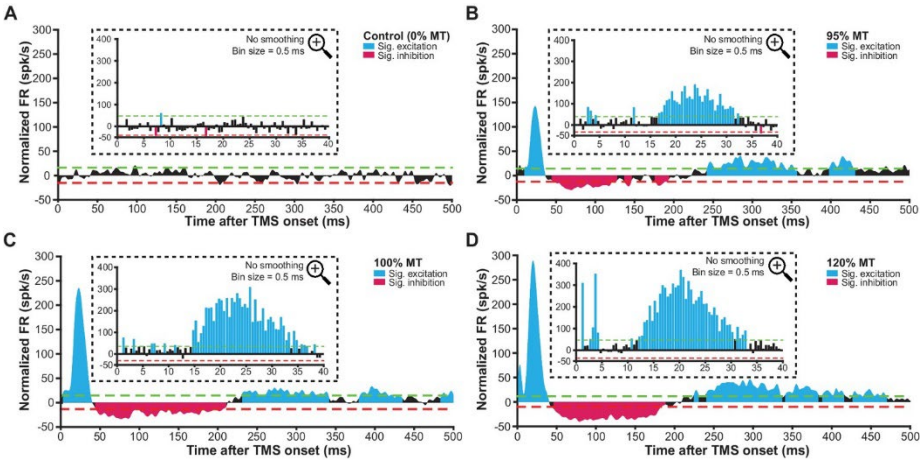

Figure 3.1 Supplement 3: Layer V neuronal response evoked by PA-oriented mspTMS at different intensities. Population average (N = 4) of normalized multiunit FR in layer V of CFA evoked by PA-oriented mspTMS. The histograms were constructed using the same procedures as those described for Figure 3.1C–F. Insets, zoom-ins (0–40 ms) on the PSTH of evoked normalized FR with no smoothing. Dashed lines, significance thresholds determined by the 2.5 or 97.5 percentile of the empirical distribution of baseline normalized FR (see Materials and methods for details). TMS was delivered at time 0 ms.

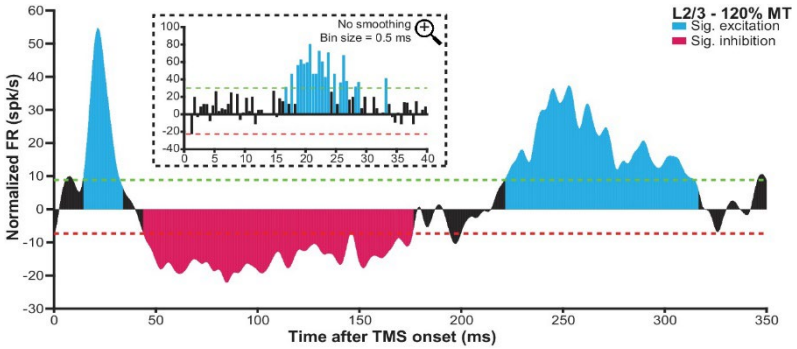

Figure 3.1 Supplement 4: mspTMS evoked a multiphasic pattern of neuronal response in layer II/III. In five animals (299 trials total), we recorded multiunit activities in layer II/III (400 μm from the cortical surface) of the CFA under mspTMS (ML orientation) at 120% MT. The histograms were constructed using the same procedures as those described for Figure 3.1C–F. The TMS-evoked multiphasic pattern of FR found here is qualitatively similar to that obtained in layer V (Figure 3.1C–F). Insets, zoom-ins (0–40 ms) on the PSTH of evoked normalized FR with no smoothing. Dashed lines, significance thresholds determined by the 2.5 or 97.5 percentile of the empirical distribution of baseline normalized FR (see Materials and methods for details). TMS was delivered at time 0 ms.

4. Investigating the circuit mechanism underlying TMS-evoked intermediate excitation

4.1 Introduction

The direct stimulation effects of TMS are limited to targets in the cerebral cortex, as the strength of electrical field induced by TMS decays rapidly as a function of distance from the TMS coil (Cohen et al., 1990; Epstein et al., 1990; Maccabee et al., 1990; Tofts and Branston, 1991). However, through synaptic mechanisms, effects of TMS can propagate to cortical and subcortical areas connected to the directly stimulated target. This was first shown in a study in which a TMS stimulus delivered to M1 unilaterally can exert an inhibitory effect on the contralateral M1 (Ferbert et al., 1992). Later neuroimaging studies utilizing EEG (Ilmoniemi et al., 1997; Komssi et al., 2002), positron emission tomography (PET) (Fox et al., 1997; Paus et al., 1997), and functional magnetic resonance imaging (fMRI) (Bestmann et al., 2004; Bohning et al., 1999) all demonstrated the indirect, synaptic mediated effects of TMS in the brain. This raise the possibility that subcortical structures not directly accessible to TMS can nonetheless be stimulated via network propagation of neural activities evoked by TMS at cortical targets.

In the previous parts of this doctoral work, a system that enables *in vivo* electrophysiological investigation of TMS-evoked activities at the level of individual neurons in laboratory animal models was developed. This opened up the opportunity to study, *in vivo*, the effect of TMS in brain circuits using the methods in systems neuroscience. We previously reported that despite its sub-millisecond duration, mspTMS targeting M1 triggers a cascade of M1 neuronal activities alternating between excitation and inhibition that lasts for 200-300 milliseconds, a phenomenon that is mediated by the propagation and effects of TMS in

neuronal network. Comparing to electrical microstimulation, which also evokes a multiphasic neuronal rhythm (Butovas and Schwarz, 2003), a surprising feature of the TMS-evoked neuronal response in M1 is the emergence of a period of excitation with a mean onset latency of 11.8 ms (95% CI: 10.2 – 13.4 ms) and a mean duration of 22.4 ms (95% CI: 17.6 – 28.1 ms; layer V recording under mspTMS inducing current in LM direction at 100% MT), a phenomenon we termed “intermediate excitation”. We showed that this period of intermediate excitation occurs in both layer V and layer II/III of M1 and it is not associated with any motor output. Interestingly, using paired-pulse TMS, human studies have shown a period of increased cortical excitability with onset and offset latencies similar to the intermediate excitation we observed (Kujirai et al., 1993; Nakamura et al., 1997; Ziemann et al., 1996). However, the origin of this excitability remains unknown. Furthermore, theta burst stimulation (TBS), a group of widely used repetitive TMS protocols for LTP or LTD induction, uses bursts of TMS pulses with an inter-pulse interval of 20 ms, corresponding also to the period of intermediate excitation. The use of 20 ms inter-pulse interval in TBS remains an empirical choice as we have little understanding in its physiological rationale. Together, all these motivate an investigation into the physiological origin of the intermediate excitation.

Although pyramidal neurons in layer V of the M1 play a central role in the generation of movement through their projections to motoneurons in the spinal cord, corticospinal projection is only a part of their output. Layer V pyramidal neurons in M1 also project directly or through the collaterals of corticospinal axons to many cerebral and sub-

cerebral targets including basal ganglia and cerebellum (Harris and Shepherd, 2015; Kita and Kita, 2011). Therefore, it is plausible that the direct activation of layer V pyramidal neurons in M1 by TMS leads to co-activations in basal ganglia and/or cerebellum that give rise to the intermediate excitation in M1 through thalamocortical projections from the motor thalamus.

Motor thalamus, which mainly consists of the ventral anterior (VA), ventral lateral (VL), and ventral medial (VM) thalamic nuclei, exerts strong control over M1 through its axonal projections (Groenewegen and Witter, 2004; Sherman and Guillery, 2006). Motor thalamus can be subdivided into two broad regions depending on its input. The basal ganglia input zone (BZ) of the motor thalamus, which includes the VA and VM nuclei, receives inputs from the output nuclei of basal ganglia, namely the globus pallidus internus (GPi) and the substantia nigra pars reticulata (SNr). Neurons in BZ project to layer I apical dendrites of M1 pyramidal neurons (Kuramoto et al., 2009), modulating the excitability of these pyramidal neurons with their somas situated in the deeper layers (Larkum et al., 2004). The cerebellum input zone (CZ) of the motor thalamus, which includes exclusively the VL nucleus, receives inputs from the deep cerebellar nuclei (DCN). It projects to M1 in a pattern that avoids layer I but targets almost exclusively layer II-V, enabling CZ neurons to directly activate pyramidal neurons these layers (Kuramoto et al., 2009).

In basal ganglia, information from the motor cortex is processed through three different pathways: the direct, indirect, and hyperdirect pathway. The end result of the processing leaves the basal ganglia

through output nuclei GPi and SNr which send out inhibitory projections to the motor thalamus. An activation of the direct pathway leads to an inhibition of the GPi and SNr, resulting in disinhibition of BZ in the motor thalamus and subsequently increased excitability in M1 (Alexander and Crutcher, 1990). On the other hand, activations of both the indirect and hyperdirect pathway excite GPi and SNr, resulting in inhibition of BZ which leads to decreased M1 excitability (Alexander and Crutcher, 1990; Nambu et al., 2002). Given this information, it can be hypothesized that the intermediate excitation can be mediated by the TMS-evoked indirect activation of the direct pathway, following the subsequent chain of neural transmission: M1 -> striatum -> GPi/SNr -> BZ -> M1 (Figure 4.1A).

In cerebellum, information from the motor cortex is relayed through the pontine nuclei (PN) in the pons and subsequently transmitted into the cerebellum through mossy fibers. Information conveyed by the mossy fibers directly reach DCN, the output structure of the cerebellum, through glutamatergic synapses (Shinoda et al., 1997). In parallel, the same information is also transmitted to granule cell for processing in the cerebellar cortex. The end result of cerebellar cortex processing is outputted by Purkinje cells which send GABAergic projections to the DCN (Ito and Yoshida, 1966). DCN, in turn, sends excitatory projections to CZ of the motor thalamus which further excites M1 (Aumann et al., 1994; Kuramoto et al., 2009). Therefore, an increase of activity in the DCN, resulted from either direct activation by mossy fibers, disinhibition of Purkinje cells, or both, can lead to increased activity in M1, offering another mechanism that can possibly mediate the intermediate excitation. However, considering the onset latency of the

intermediate excitation, it is unlikely that microcircuits in the cerebellar cortex are involved as these circuits involve complex polysynaptic pathways. For this reason, we hypothesize that the intermediate excitation can also be a result of TMS-evoked indirection activation of the DCN through mossy fibers, following the subsequent chain of neural transmission: M1 -> pontine nuclei -> DCN -> CZ -> M1 (Figure 4.1B).

In the following part of this doctoral work, we examined the two aforementioned hypotheses by conducting simultaneous TMS and extracellular electrophysiology recording in BZ and CZ of the motor thalamus in anesthetized rats. If either hypothesis is true, a phase of excitatory activities shall commence in BZ or CZ 1-2 ms prior to the onset of the intermediate excitation in M1, as one would expect given the typical synaptic latency in the mammalian cortex (Boudkkazi et al., 2007).

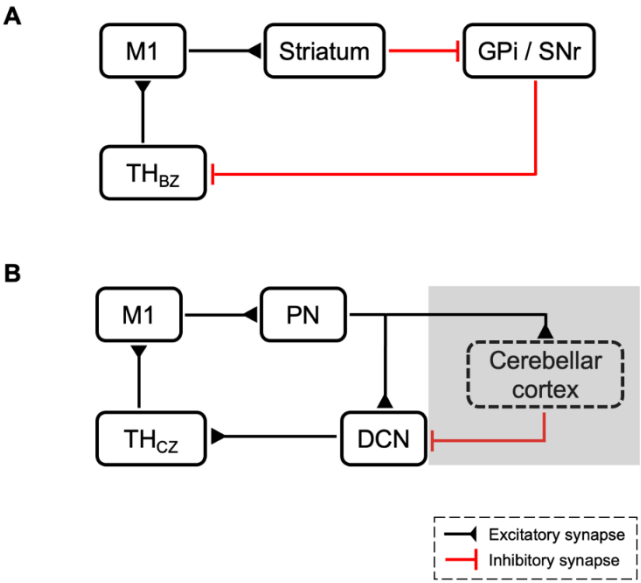

Figure 4.1: Hypothesized circuit mechanisms that mediate the intermediate excitation. (A) Cortico-basal ganglia-thalamo-cortico loop. **(B)** Cortico-cerebello-thalamo-cortical loop. The shaded region indicates the loop branch that involves the cerebellar cortex, which is deemed unlikely given the onset latency of intermediate excitation. Abbreviations: *M1*, primary motor cortex. *GPi*, globus pallidus internus. *SNr*, substantia nigra pars reticulata. TH_{BZ}, the basal ganglia input zone of motor thalamus. *PN*, pontine nuclei. *DCN*, deep cerebellum nuclei. TH_{CZ}, the cerebellar input zone of motor thalamus.

4.2 Results

In ketamine-xylazine anesthetized adult male Sprague-Dawley rats, we recorded extracellular electrophysiology in the BZ (N = 6) and the CZ (N = 8) of the motor thalamus as we delivered monophasic single-pulse TMS (mspTMS) to the primary forelimb motor area (caudal forelimb area, CFA) at the intensity of 100% and 120% of motor threshold (MT). An electrolytic lesion was made at the end of each experiment to mark the location of the recording. The delineation of BZ (VA and VM nuclei) and CZ (VL nucleus) in rats has been described in

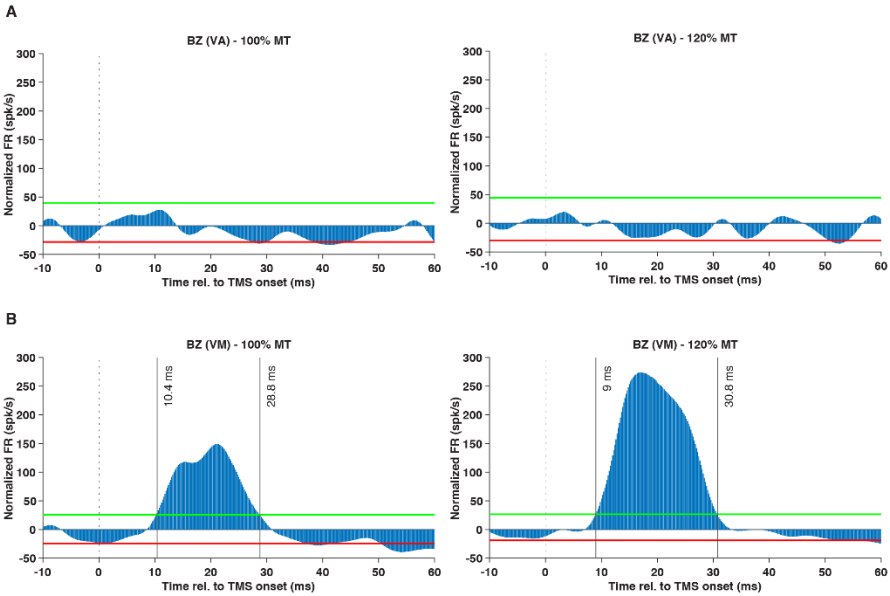

Figure 4.2: Examples of intermediate excitation in BZ. PSTHs of normalized multiunit FR in the VA **(A)** and the VM **(B)** nucleus of BZ evoked by ML-oriented mspTMS of increasing intensity delivered to CFA. The PSTHs were smoothed by a Gaussian kernel (σ = 2 ms) for visualization. Vertical dash lines, the time of TMS onset. Colored lines, significance thresholds determined by the 2.5 (red) or 97.5 (green) percentile of the empirical distribution of baseline normalized FR. Vertical solid lines, the onset and offset latency of intermediate excitation (see Materials and Methods for details).

the literature based on immunochemical staining against GAD67 and VGluT2 (Nakamura et al., 2014). We verified this in our animals (Supplementary Figure S1) and used this information to assign recording locations to one of the two areas.

In BZ, we observed two different types of response. In the anterior part of the BZ, the ventral anterior (VA) nucleus, mspTMS at 100% and 120% MT evoked no intermediate excitation after TMS onset (Fig. 4.2A; N=3). In the posterior part of the BZ, the ventral medial (VM) nucleus, mspTMS at 100% MT evoked intermediate excitation with a

mean onset latency of 11.4 ms (95% CI: 9.9 – 14.2 ms) and a duration of 20.8 ms (95% CI: 15.2 – 30.4 ms). At 120% MT, the onset latency and duration were 10.1 (95% CI: 8.5 – 13 ms) and 23.3 ms (95% CI: 17.3 – 33 ms), respectively (Fig. 4.2B; N=3).

In CZ, we reliably observed intermediate excitation in the first tens of milliseconds after TMS onset. At 100% MT, the mean onset latency of the intermediate excitation was 12.6 ms (95% CI: 8.2 – 20.1) and the mean duration was 25.1 ms (95% CI: 18.2 – 34.2 ms). At 120% MT, the mean onset latency and duration were 10.2 ms (95% CI: 6.2 – 16.7 ms) and 27.7 ms (95% CI: 20.4 – 36.6 ms), respectively. As indicated by the wide range of its confidence interval, onset latency of the intermediate excitation in CZ showed considerable variation. Among the 8 animals measured, at 100% MT, we observed 2 cases with an onset latency $\leqslant$ 5 ms (Fig. 4.3A), 4 cases with an onset latency between 5 and 15 ms (Fig. 4.3B), and 2 cases with an onset latency $\geqslant$ 15 ms (Fig. 4.3C). At 120% MT, the number of cases for the three groups changed to 3, 3, and 2.

In Figure 4.4, we summarize data from this study and compare it with the results obtained in M1 from the study reported in the Section 3 of this doctoral work. It can be seen that while the intermediate excitation was not detectable in the anterior part of BZ (the VA nucleus), it was detected in the posterior part of BZ (the VM nucleus) and in CZ (the VL nucleus). In VM of BZ, at 100% MT, intermediate excitation displayed a mean onset latency that is 0.6 ms earlier than that in M1 (mean = 11.8 ms, 95% CI: 10.2 – 13.4 ms) but this difference is not statistically significant (p=0.77, difference of group means using bootstrapping;

same for the comparisons below). At 120% MT, the mean onset latency is 1.2 ms later than that observed in M1 (mean = 9.0 ms, 95% CI: 7.3 – 10.6 ms) and the difference is not statistically significant (p=0.48). In VL of CZ, at 100% MT, the mean onset latency of intermediate excitation is 0.8 ms later than that in M1 and the difference is not statistically significant (p=0.81). At 120% MT, the mean onset latency is 1.2 ms later than that in M1 and the difference is also not statistically significant (p=0.66).

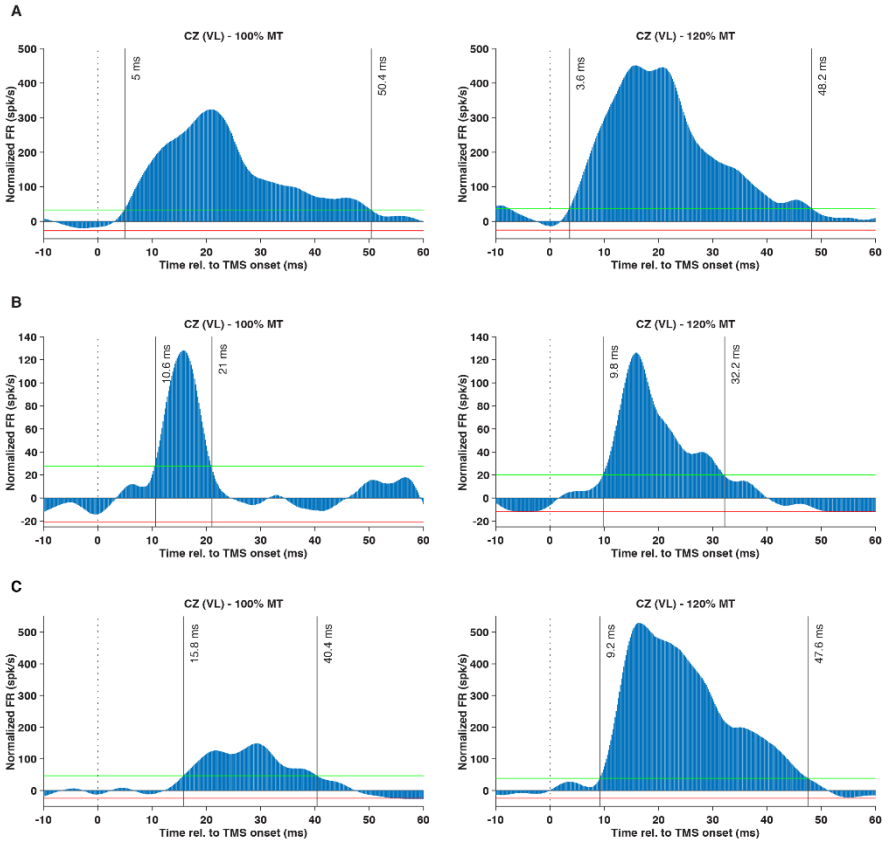

Figure 4.3: Examples of intermediate excitation in CZ. PSTHs of normalized multiunit FR in the VL nucleus of CZ evoked by ML-oriented mspTMS of increasing intensity delivered to CFA, illustrating a heterogenous onset pattern of the intermediate excitation in CZ: **(A)** early onset, **(B)** normal onset, and **(C)** late onset. Symbols are the same as those in Fig. 4.2.

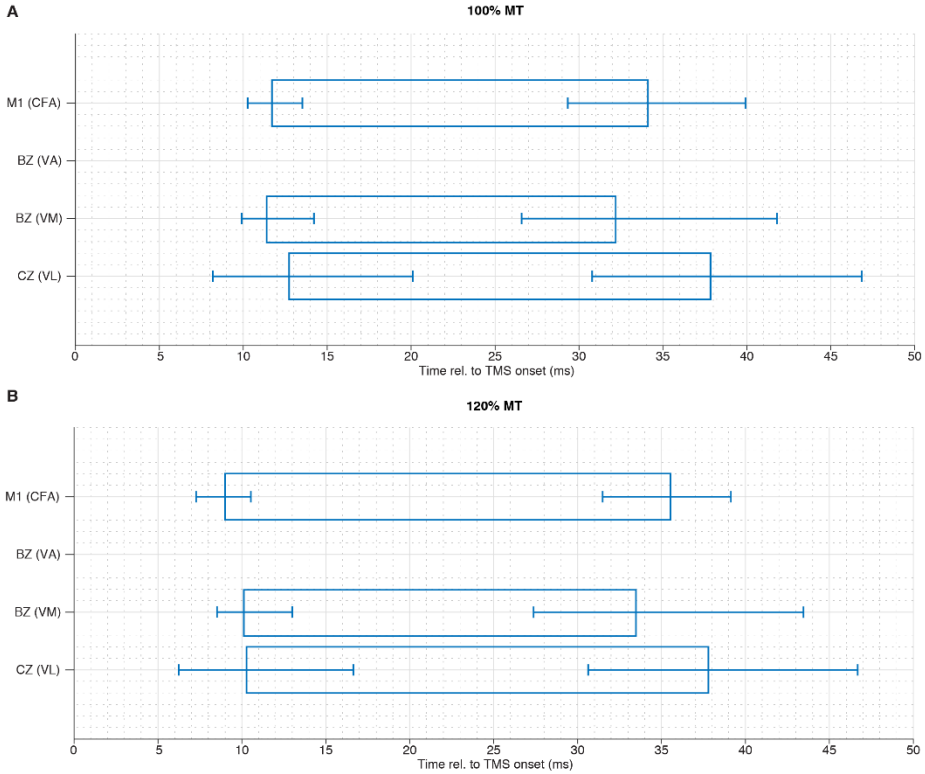

Figure 4.4: Comparing the timing of intermediate excitation in M1, BZ, and CZ. The onset and offset latency of intermediate excitation evoked by mspTMS at 100% MT **(A)** and 120% MT **(B)** detected in the CFA of M1 (N=19), the VA and VM nucleus of BZ (N=6; 3 in each nucleus), and the VL nucleus of CZ (N=8). Error bars signify bootstrapped 95% confidence interval.

4.3 Discussion

In this study, we measured in motor thalamus extracellular neuronal activities evoked by medial-lateral oriented mspTMS delivered to the forelimb area of M1 in ketamine-xylazine anesthetized rats. We hypothesized that if the intermediate excitation observed in our previous M1 study was mediated by activations in the cortico-basal ganglia-thalamo-cortical (CBGTC) or the cortico-cerebello-thalamo-cortical (CCTC) loop, we would observe intermediate excitation in the basal ganglia input zone (BZ) or the cerebellum input zone (CZ) of the motor thalamus with an onset latency that is earlier than that of the M1 intermediate excitation by one synaptic delay (1-2 ms). Our results did not confirm either of the two hypotheses. In BZ, we detected two types of response: in VA nucleus, intermediate excitation was not detected while in VM nucleus, intermediate excitation was detected but its average onset latency is not significantly different than that in M1. In CZ, intermediate excitation was detected; however, its onset latency displayed a large degree of variation, and the average is also not significantly different from its M1 counterpart.

It is intriguing that in BZ, intermediate excitation was only detected in VM but not VA nucleus. Although both VM and VA receive strong GABAergic inputs from basal ganglia, VA projects exclusively to motor cortices while VM projects to motor as well as other cortical areas, including the orbital, cingulate, and visual cortex (Kuramoto et al., 2015). Therefore, the two BZ nuclei likely represent two different output channels of basal ganglia forming two parallel branches of the CBGTC loop. In this study, the average onset latency of intermediate excitation

in VM at 100% MT is 0.6 ms earlier than the average onset in M1 found in our earlier study. The difference did not reach statistical significance, a result that might be due to limited statistical power given the limited sample size of the VM data (N=3). Nonetheless, the result suggests that VM and its associated branch of the CBGTC loop remain a candidate that may mediate intermediate excitation in M1. A follow-up study in VM is needed to evaluate this possibility, ideally using simultaneous recording in M1 and VM that enables the direct cortex-thalamus comparison and eliminates between-animals variance.

In CZ, we observed a heterogeneous onset pattern of intermediate excitation, including cases of early (<5 ms) onset as well as cases of late (>15 ms) onset. It is plausible that this heterogeneity is a result of functional compartmentalization within the CZ. Anatomical evidence from mice suggests that while VA and VM nuclei of BZ does not receive projections from layer V pyramidal neurons in M1, the dorsal-posterior portion of the VL nucleus of CZ does receive such projections and the projection strength displays a descending gradient in the anterior-posterior direction (Jeong et al., 2016). Therefore, it can be speculated that cases of intermediate excitation with an early onset were resulted from recording at CZ locations that receive strong corticothalamic input. As TMS activates layer V pyramidal neurons in M1 and their associated corticothalamic projections, excitatory activities can be expected at these VL locations in the first few milliseconds after TMS onset, followed by excitatory neuronal activities conducted in the CCTC loop. A similar speculation can be made for the cases of intermediate excitation with a late onset. It is known from non-human primate work

that CZ can be divided into multiple sub-regions that receive input from different parts of the DCN and these sub-regions in turn project to different cortical targets, representing different cerebellar output channels (Dum and Strick, 2003; Percheron et al., 1996). Therefore, for cases of intermediate excitation with a late onset, it is possible that those recordings were carried out in sub-regions of the VM that are not part of the fast cerebellar conduction pathway that bypasses the cerebellar cortex as hypothesized in this study. All these considerations highlight the need for further investigation in CZ with a careful consideration of its functional compartmentalization. Furthermore, the possible roles of brain state in the onset variability of CZ intermediate excitation also warrants consideration, and it can be best addressed by adopting simultaneous M1 and CZ recording.

For future studies, it is also worth exploring other possible neural circuits that may underlie the intermediate excitation. In addition to the projection targets considered in this study, neurons in the layer V of M1 also project to many other subcortical and cortical targets, including the paracentral, central lateral, and parafasicular nuclei of the thalamus, zona incerta and fields of forel of the hypothalamus, reticular formation of the midbrain, secondary motor cortex and somatosensory cortex of the ipsilateral side, and the primary motor cortex of the contralateral side (Jeong et al., 2016; Oswald et al., 2013). All these structures could potentially play a role in the generation of intermediate excitation, and they shall be considered should further examinations of the CBGTC and CCTC loops return null results that conclusively reject the involvement of these two loops.

Furthermore, is shall be noted that in several animals, due to errors in electrode placement, we recorded TMS-evoked response in ventral posteromedial nucleus (VPM; n=2), paracentral nucleus (PC; N=1), posterior nucleus (PO; N=2), and ventral submedius nucleus (SubV; N=1), all of which are sensory relay nuclei in the thalamus. Interestingly, in these nuclei, we observed a mean onset of the intermediate excitation at 8.8 ms (95% CI: 4.4 – 15.0 ms) for 100% MT stimuli and at 4.3 ms (95% CI: 1.9 – 7.7 ms) for 120% MT stimuli. This unexpected finding raised the question of whether the sensory component of a TMS pulse plays any role in the generation of the intermediate excitation. It is also highly of interests for future studies to examine this possibility.

4.4 Materials and Methods

4.4.1 Animals

Identical to 2.4.3 except animal N = 14.

4.4.2 Surgery

Identical to 2.4.4 except a 3x3 mm craniotomy was made over the left sensorimotor cortex. The resulted trepanation extended from −1 mm to -4 mm to bregma and from 0.5 mm to 3.5 mm lateral relative to the midline.

4.4.3 Transcranial magnetic stimulation (TMS)

Identical to 2.4.5.

4.4.4 Extracellular electrophysiology (EEP)

EEP was recorded through a pair (signal-reference) of microelectrodes (ca. 1.5 MΩ impedance at 1 kHz) fabricated in-house from glass-coated platinum-tungsten wires (Thomas RECORDING, Giessen, Germany). A thin silver wire with silver-chloride coating was used as the ground electrode. The three electrodes were arranged in a three-pronged fashion to minimize the induction loop area between them. The assembly was held by a non-conductive non-magnetic L-shape holder that was mounted on a micropositioner (David Kopf Instruments, Tujunga, USA). The recording electrode was lowered, through the cranial window, into BZ or CZ according to stereotaxic coordinates reported in the literature (Nakamura et al., 2014; Paxinos and Watson, 2006) and validated in 2 of our cohort of animals (Supplementary figure S1). Specifically, for BZ, the VA nucleus was targeted at [-2.2, 1.4, 7.0 mm] (anterior-posterior relative to bregma, medial-lateral relative to midline, dorsal-ventral relative to brain surface; the same in the following), the VM nucleus was targeted at [-3.2, 1.4, 7.0 mm]; for CZ, the VL nucleus was targeted at [-3.0, 1.4, 6.6 mm]. The reference electrode was also lowered into the brain but outside the boundary of BZ and CZ. The ground electrode was positioned to be in contact with unresected subcutaneous tissue by the border of the cranial window. Signals from the electrodes were transmitted through a set of 36-gauge low-noise miniature coaxial cables (Axon' Cable S.A.S., Montmirail, France) to our TMS-EEP amplifier as described in details in Chapter 2. The signal from the amplifier output was digitized (USB-ME64-System,

MultiChannel Systems GmbH, Reutlingen, Germany) at 40 kHz and subsequently visualized and stored on a PC for analysis.

4.4.5 Histology

Identical to 3.4.7.

4.4.6 Immunohistochemistry

To validate the delineation of BZ and CZ reported by Nakamura et al. (2014), in 8 animals, we performed immunohistochemistry staining against VGluT2 and GAD67 in sections adjacent to lesion locations containing motor thalamus. To inactivate the endogenous peroxidases, sections were incubated in 0.1% H_2O_2 solution in PBS for 20 min at 4°C. To saturate nonspecific binding, the sections were incubated in 10% normal serum depending on the species from which the secondary antibody was derived (goat or donkey; Vector Laboratories, Inc.; USA) for 1 h at room temperature (RT). After saturation of nonspecific binding, the sections were incubated for 13-16 h in a humidity chamber at RT with a mixture of antibodies against VGluT2 (1:1000; VGluT2-135402, Synaptic Systems, Germany) and GAD67 (1:1000; clone 1G10.2; Merck, Germany) in 0.2% Triton-PBS containing 1% v/v donkey serum. After washing, the sections were incubated for 4h with a mixture of fluorophore-conjugated secondary antibodies: Alexa Fluor 488 donkey anti-rabbit IgG (1:400 for 2.5h at RT; Invitrogen, Thermo Fischer Scientific, USA), and Alex Fluor 647 goat anti-mouse IgG (1:400 for 2.5h at RT; Invitrogen, Thermo Fischer Scientific, USA). Fluorescently labeled sections were mounted on glass slides, cover-slipped, and

examined under a confocal microscope (Zeiss, Germany). BZ and CZ were identified in the sections based on florescence and this information was used subsequently in all other animals to classify lesion-marked recording sites to BZ or CZ.

4.4.7 Quantification and statistical analysis

Data processing methods are identical to those described in 3.4.8.

Statistical analysis was performed using bootstrapping-based methods. Confidence interval for the mean was determined based on the distribution of the means of the resampled data (n = 10000 with replacement; same below). Statistical difference between means of two groups was determined by the probability of obtaining the actual mean difference given the distribution of mean differences based on resampled data. Threshold for statistical significance was set at $p < 0.05$.

4.5 Contributions

Bingshuo Li: conceptualization, data curation, data analysis, writing – original draft, writing – review and editing;

Alia Benali: conceptualization, data curation, data analysis, writing – original draft, writing – review and editing, daily supervision;

Cornelius Schwarz: laboratory resources, funding, data interpretation, writing – review and editing, supervision;

Martin Giese: laboratory resources, funding, data interpretation, supervision;

Ulf Ziemann: laboratory resources, funding, data interpretation, supervision.

4.6 Supplementary Information

Figure S1: Delineation of BZ and CZ based on immunohistochemical staining. A parasagittal section 1.35 mm to the midline was stained against GAD67 and VGluT2, and subsequently labeled with secondary antibodies conjugated with Alexa Fluor 647 (red) and Alex Fluor 488 (green), respectively. Borders between BZ and CZ were drawn in the motor thalamus based on the pattern of florescence.

5. Conclusion

Reaching the brain noninvasively with a brief and painless magnetic pulse, TMS revolutionized brain stimulation, a field which had been characterized by methods involving invasive procedures and high level of discomfort. TMS has become the method-of-choice for brain stimulation in a wide range of scientific and clinical context that spans from the study of cortical microcircuits to the management of psychiatric disorders. However, despite its many exciting developments and fast-rising popularity, TMS is poorly understood physiologically. Although we know that TMS can produce various behavioral outcomes in humans, we know very little of its neurophysiological underpinnings. This inadequacy is largely resulted from the difficulty of studying neuronal activities under the tesla-level strong magnetic pulse of TMS, something that had been considered as impossible until now.

In this doctoral work, an experimental platform on which TMS can be investigated *in vivo* in laboratory animals using extracellular electrophysiology was developed. The success of this development relied on the simultaneous attenuation of magnetic, electric, and acoustic interference and inadvertent charge injection. It allows nearly interruption-free extracellular electrophysiology recording under high-intensity single or repetitive TMS stimuli. This methodological advance enabled *in vivo* research of the neurophysiology of TMS and the neurophysiology-driven development of novel TMS therapeutic interventions. It is widely accessible for the research community (open-source license CC BY 4.0) and is easy to implement. Despite the success, in my view, an upscaling of the platform to allow data acquisition from multiple channels is much needed as it is crucial to

monitor simultaneously as many neurons and brain locations as possible to understand the dynamics of neural circuits. A multichannel upgrade will bring a multitude of challenges in electronic design; however, the technical principles uncovered in this work set down a solid foundation for this future development.

The experimental work in M1 provided the very first description of neuronal spiking activities in the output layer of M1 evoked by mspTMS. A single TMS pulse lasting no more than half of a millisecond evokes a long-lasting cascade of neuronal activities consists of an early excitation phase (< 6 ms), an intermediate excitation phase (8-26 ms), an inhibition phase (33-172 ms), and a late excitation phase (199-290 ms). Although not tested explicitly in this study, the observed multiphasic activities can readily be related to various known phenomena in human TMS (see Fig. 5.1 for a summary). The early excitation phase, characterized by spiking activities at 1-1.5 ms and 2.5-4.5 ms post-TMS (Fig. 3.2), captured the high-frequency activation of layer V neurons that may share the same mechanisms as I-wave generation reported in cats (Patton and Amassian, 1954), monkeys (Amassian et al., 1987) and humans (Di Lazzaro et al., 2012), and may offer a neuronal explanation for the short interval intracortical facilitation (Ziemann et al., 1998), obtained in a human paired-pulse TMS protocol. The intermediate excitation phase, given its latency, duration, presence in both layer V and II/III and its apparent lack of motor output, reflects a high excitability state of the motor cortex. This excitation may be a result of post-inhibitory rebound (Adhikari et al., 2012) as TMS-evoked fast $GABA_A$ activity that synchronized pyramidal neurons for their initial high-

frequency activation comes to an end, or a result of intracortical or cortical-subcortical interactions. The neural mechanism of TMS protocols such as intracortical facilitation (Ziemann et al., 1996) and theta burst stimulation (inter-pulse interval of 20 ms within each burst) (Benali et al., 2011; Suppa et al., 2016) remain unknown; however, it is likely that these protocols exploit this particular phase of excitation for their physiological effects. The long-lasting inhibition phase that follows the second excitation is well-known, and evidence supports the notion that it is mediated by $GABA_B$ (Butovas et al., 2006; Murphy et al., 2016) and it underlies the long-interval intracortical inhibition as well as the cortical silent period in human TMS (McDonnell et al., 2006; Stetkarova and Kofler, 2013; Valls-Solé et al., 1992). The late excitation phase, occurring after the inhibition, represents a period of rebound excitation most likely resulting from the termination of $GABA_B$ inhibition, and corresponds to the late cortical disinhibition, which has been used for augmenting plasticity induction in human TMS (Cash et al., 2016). Additionally, periodicity (ca. 15 Hz) in neuronal firing was observed in the late excitation phase, a phenomenon that could give rise to TMS-evoked oscillations as reported in human TMS-EEG (Rosanova et al., 2009). Future studies may leverage the technology developed in this project to examine the causal relationship between different phases of evoked neuronal activities and these human TMS phenomena and to elucidate their underlying long- or short-distance circuit mechanisms. TMS stimulates the cortical layers of the brain. However, the impact of this stimulation propagates into deeper brain structures and modulates their functional networks. This brings the possibility to harvest the network

effects of TMS for therapeutic purposes. It is therefore of interest to understand the network propagation of TMS in various deep-brain functional networks.

In the last part of this doctoral work, I explored this topic by examining possible circuit mechanisms that give rise to the TMS-evoked intermediate excitation in M1. It was hypothesized that activations in the cortico-basal ganglia-thalamo-cortical (CGBTC) or the cortico-cerebello-thalamo-cortical (CCTC) loop are involved in the genesis of intermediate excitation. TMS-EEP recordings were carried out in the basal ganglia input zone (BZ) and cerebellum input zone (CZ) of the motor thalamus.

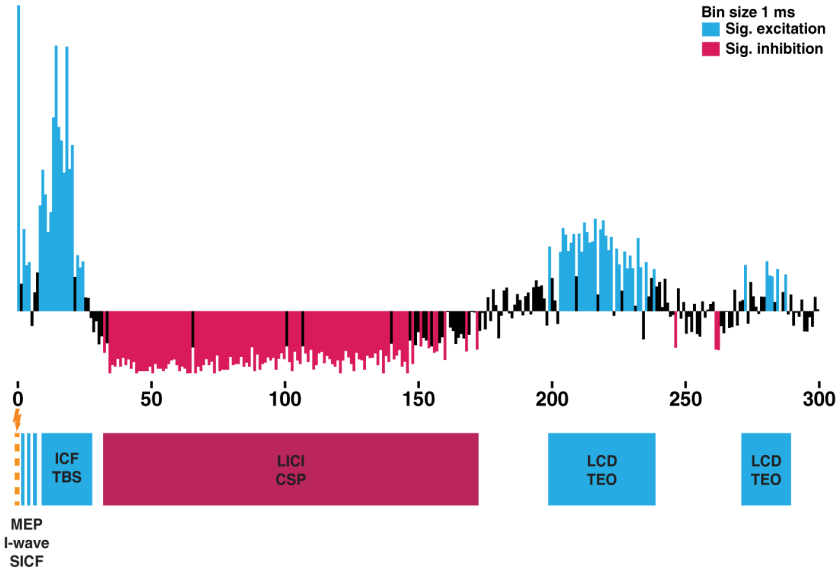

Figure 5.1 Temporal relations between TMS-evoked M1 layer V spiking activities and various known human TMS phenomena. CSP, cortical silent period; ICF, intracortical facilitation; LCD, late cortical disinhibition; LICI, long-interval intracortical inhibition; MEP, motor-evoked potential; SICF, short-interval intracortical facilitation; TEO, TMS-evoked oscillation.

Should CGBTC or CCTC loop be involved, excitatory neuronal activities shall be observed in BZ or CZ at a latency that is 1 synaptic delay earlier than the onset latency of intermediate excitation in M1. Data collected in these recordings did not allow clear conclusions on these hypotheses to be drawn due to limited statistical power. Nonetheless, it confirmed the existence of intermediate excitation outside of M1 and highlighted the need to examine different sub-compartments of BZ and CZ, to consider other cortex-originated long-distance circuits, and to consider the possible roles of TMS-associated sensory inputs in the generation of the intermediate excitation.

In conclusion, in this doctoral work, a system that allows near artifact-free extracellular electrophysiology recording under TMS was developed. Leveraging this technical advance, TMS-evoked neuronal activities in M1 were revealed for the first time, and circuit-based TMS propagation was examined in the CGBTC and CCTC loops. It is my anticipation that future work will expand the recording system for multichannel support and further examine in detail the effects of various TMS stimuli in cortical and sub-cortical networks, endeavors that will be of high importance for the development of novel and effective TMS therapeutics.

6. References

Adhikari, M.H., Quilichini, P.P., Roy, D., Jirsa, V., and Bernard, C. (2012). Brain State Dependent Postinhibitory Rebound in Entorhinal Cortex Interneurons. J. Neurosci. *32*, 6501–6510.

Alexander, G.E., and Crutcher, M.D. (1990). Functional architecture of basal ganglia circuits: neural substrates of parallel processing. Trends Neurosci. *13*, 266–271.

Allen, E.A., Pasley, B.N., Duong, T., and Freeman, R.D. (2007). Transcranial magnetic stimulation elicits coupled neural and hemodynamic consequences. Science *317*, 1918–1921.

Amassian, V.E., and Stewart, M. (2003). Motor cortical and other cortical interneuronal networks that generate very high frequency waves. Suppl. Clin. Neurophysiol. *56*, 119–142.

Amassian, V.E., Stewart, M., Quirk, G.J., and Rosenthal, J.L. (1987). Physiological basis of motor effects of a transient stimulus to cerebral cortex. Neurosurgery *20*, 74–93.

Amassian, V.E., Quirk, G.J., and Stewart, M. (1990). A comparison of corticospinal activation by magnetic coil and electrical stimulation of monkey motor cortex. Electroencephalogr. Clin. Neurophysiol. *77*, 390–401.

Asanuma, H., and Rosén, I. (1973). Spread of mono- and polysynaptic connections within cat's motor cortex. Exp. Brain Res. *16*, 507–520.

Aumann, T.D., Rawson, J.A., Finkelstein, D.I., and Horne, M.K. (1994). Projections from the lateral and interposed cerebellar nuclei to the thalamus of the rat: a light and electron microscopic study using single and double anterograde labelling. J. Comp. Neurol. *349*, 165–181.

Aydin-Abidin, S., Trippe, J., Funke, K., Eysel, U.T., and Benali, A. (2008). High- and low-frequency repetitive transcranial magnetic stimulation differentially activates c-Fos and zif268 protein expression in the rat brain. Exp Brain Res *188*, 249–261.

Barker, A.T., Jalinous, R., and Freeston, I.L. (1985). Non-invasive magnetic stimulation of human motor cortex. Lancet (London, England) *1*, 1106–1107.

Bates, D., Mächler, M., Bolker, B., and Walker, S. (2015). Fitting Linear Mixed-Effects Models Using lme4. J. Stat. Softw. *67*.

Benali, A., Trippe, J., Weiler, E., Mix, A., Petrasch-Parwez, E., Girzalsky, W., Eysel, U.T., Erdmann, R., and Funke, K. (2011). Theta-burst transcranial magnetic stimulation alters cortical inhibition. J Neurosci *31*, 1193–1203.

Bestmann, S., Baudewig, J., Siebner, H.R., Rothwell, J.C., and Frahm, J. (2004). Functional MRI of the immediate impact of transcranial magnetic stimulation on cortical and subcortical motor circuits. Eur. J. Neurosci. *19*, 1950–1962.

Bohning, D.E., Shastri, A., McConnell, K.A., Nahas, Z., Lorberbaum, J.P., Roberts, D.R., Teneback, C., Vincent, D.J., and George, M.S. (1999). A combined TMS/fMRI study of intensity-dependent TMS over motor cortex. Biol. Psychiatry *45*, 385–394.

Boudkkazi, S., Carlier, E., Ankri, N., Caillard, O., Giraud, P., Fronzaroli-Molinieres, L., and Debanne, D. (2007). Release-dependent variations in synaptic latency: a putative code for short- and long-term synaptic dynamics. Neuron *56*, 1048–1060.

Bungert, A., Antunes, A., Espenhahn, S., and Thielscher, A.

(2016). Where does TMS Stimulate the Motor Cortex? Combining Electrophysiological Measurements and Realistic Field Estimates to Reveal the Affected Cortex Position. Cereb. Cortex 1–12.

Butovas, S., and Schwarz, C. (2003). Spatiotemporal effects of microstimulation in rat neocortex: a parametric study using multielectrode recordings. J. Neurophysiol. *90*, 3024–3039.

Butovas, S., Hormuzdi, S.G., Monyer, H., and Schwarz, C. (2006). Effects of electrically coupled inhibitory networks on local neuronal responses to intracortical microstimulation. J. Neurophysiol. *96*, 1227–1236.

Buzsáki, G. (2004). Large-scale recording of neuronal ensembles. Nat. Neurosci. *7*, 446–451.

Cash, R.F.H., Murakami, T., Chen, R., Thickbroom, G.W., and Ziemann, U. (2016). Augmenting Plasticity Induction in Human Motor Cortex by Disinhibition Stimulation. Cereb. Cortex *26*, 58–69.

Chen, R., Classen, J., Gerloff, C., Celnik, P., Wassermann, E.M., Hallett, M., and Cohen, L.G. (1997). Depression of motor cortex excitability by low-frequency transcranial magnetic stimulation. Neurology *48*, 1398–1403.

Chung, S.W., Rogasch, N.C., Hoy, K.E., and Fitzgerald, P.B. (2015). Measuring brain stimulation induced changes in cortical properties using TMS-EEG. Brain Stimul. *8*, 1010–1020.

Cohen, L.G., Roth, B.J., Nilsson, J., Dang, N., Panizza, M., Bandinelli, S., Friauf, W., and Hallett, M. (1990). Effects of coil design on delivery of focal magnetic stimulation. Technical considerations. Electroencephalogr. Clin. Neurophysiol. *75*, 350–357.

Cohen, L.G., Ziemann, U., Chen, R., Classen, J., Hallett, M., Gerloff, C., and Butefisch, C. (1998). Studies of neuroplasticity with transcranial magnetic stimulation. J. Clin. Neurophysiol. *15*, 305–324.

Deffeyes, J.E., Touvykine, B., Quessy, S., and Dancause, N. (2015). Interactions between rostral and caudal cortical motor areas in the rat. J. Neurophysiol. *113*, 3893–3904.

Dum, R.P., and Strick, P.L. (2003). An unfolded map of the cerebellar dentate nucleus and its projections to the cerebral cortex. J. Neurophysiol. *89*, 634–639.

Ecker, A.S., Berens, P., Cotton, R.J., Subramaniyan, M., Denfield, G.H., Cadwell, C.R., Smirnakis, S.M., Bethge, M., and Tolias, A.S. (2014). State dependence of noise correlations in macaque primary visual cortex. Neuron *82*, 235–248.

Epstein, C.M., Schwartzberg, D.G., Davey, K.R., and Sudderth, D.B. (1990). Localizing the site of magnetic brain stimulation in humans. Neurology *40*, 666–670.

Esser, S.K., Hill, S.L., and Tononi, G. (2005). Modeling the effects of transcranial magnetic stimulation on cortical circuits. J. Neurophysiol. *94*, 622–639.

Ferbert, A., Priori, A., Rothwell, J.C., Day, B.L., Colebatch, J.G., and Marsden, C.D. (1992). Interhemispheric inhibition of the human motor cortex. J. Physiol. *453*, 525–546.

Fowler, E.P. (1976). Microphony of coaxial cables. Proc. Inst. Electr. Eng. *123*, 1043–1046.

Fox, P., Ingham, R., George, M.S., Mayberg, H., Ingham, J., Roby, J., Martin, C., and Jerabek, P. (1997). Imaging human intra-

cerebral connectivity by PET during TMS. Neuroreport *8*, 2787–2791.

Fox, P.T., Narayana, S., Tandon, N., Sandoval, H., Fox, S.P., Kochunov, P., and Lancaster, J.L. (2004). Column-based model of electric field excitation of cerebral cortex. Hum. Brain Mapp. *22*, 1–14.

Funke, K., and Benali, A. (2010). Cortical cellular actions of transcranial magnetic stimulation. Restor. Neurol. Neurosci. *28*, 399–417.

Groenewegen, H.J., and Witter, M.P. (2004). Thalamus. In The Rat Nervous System, G. Paxinos, ed. (Elsevier), pp. 407–453.

Halekoh, U., and Hoejsgaard, S. (2014). A Kenward-Roger Approximation and Parametric Bootstrap Methods for Tests in Linear Mixed Models - The R Package pbkrtest. J. Stat. Softw. *59*.

Harris, K.D., and Shepherd, G.M.G. (2015). The neocortical circuit: themes and variations. Nat. Neurosci. *18*, 170–181.

Hess, C.W., Mills, K.R., and Murray, N.M. (1987). Responses in small hand muscles from magnetic stimulation of the human brain. J. Physiol. *388*, 397–419.

Huang, Y.Z., Edwards, M.J., Rounis, E., Bhatia, K.P., and Rothwell, J.C. (2005). Theta burst stimulation of the human motor cortex. Neuron *45*, 201–206.

Ilmoniemi, R.J., Virtanen, J., Ruohonen, J., Karhu, J., Aronen, H.J., Näätänen, R., and Katila, T. (1997). Neuronal responses to magnetic stimulation reveal cortical reactivity and connectivity. Neuroreport *8*, 3537–3540.

Ito, M., and Yoshida, M. (1966). The origin of cerebellar-induced inhibition of Deiters neurones. I. Monosynaptic initiation of the inhibitory

postsynaptic potentials. Exp. Brain Res. *2*, 330–349.

Jeong, M., Kim, Y., Kim, J., Ferrante, D.D., Mitra, P.P., Osten, P., and Kim, D. (2016). Comparative three-dimensional connectome map of motor cortical projections in the mouse brain. Sci. Rep. *6*, 20072.

Kaneko, K., Kawai, S., Fuchigami, Y., Morita, H., and Ofuji, A. (1996). The effect of current direction induced by transcranial magnetic stimulation on the corticospinal excitability in human brain. Electroencephalogr. Clin. Neurophysiol. *101*, 478–482.

Kernell, D., and Chien-Ping, W.U. (1967). Responses of the pyramidal tract to stimulation of the baboon's motor cortex. J. Physiol. *191*, 653–672.

Kita, H., and Kita, T. (2011). Cortical Stimulation Evokes Abnormal Responses in the Dopamine-Depleted Rat Basal Ganglia. J. Neurosci. *31*, 10311–10322.

Kita, T., and Kita, H. (2012). The subthalamic nucleus is one of multiple innervation sites for long-range corticofugal axons: a single-axon tracing study in the rat. J. Neurosci. *32*, 5990–5999.

Komssi, S., Aronen, H.J., Huttunen, J., Kesäniemi, M., Soinne, L., Nikouline, V. V, Ollikainen, M., Roine, R.O., Karhu, J., Savolainen, S., et al. (2002). Ipsi- and contralateral EEG reactions to transcranial magnetic stimulation. Clin. Neurophysiol. *113*, 175–184.

Kozyrev, V., Eysel, U.T., and Jancke, D. (2014). Voltage-sensitive dye imaging of transcranial magnetic stimulation-induced intracortical dynamics. Proc. Natl. Acad. Sci. U. S. A. *111*, 13553–13558.

Kujirai, T., Caramia, M.D., Rothwell, J.C., Day, B.L., Thompson, P.D., Ferbert, A., Wroe, S., Asselman, P., and Marsden, C.D. (1993).

Corticocortical inhibition in human motor cortex. J. Physiol. *471*, 501–519.

Kuramoto, E., Furuta, T., Nakamura, K.C., Unzai, T., Hioki, H., and Kaneko, T. (2009). Two types of thalamocortical projections from the motor thalamic nuclei of the rat: A single neuron-tracing study using viral vectors. Cereb. Cortex *19*, 2065–2077.

Kuramoto, E., Ohno, S., Furuta, T., Unzai, T., Tanaka, Y.R., Hioki, H., and Kaneko, T. (2015). Ventral medial nucleus neurons send thalamocortical afferents more widely and more preferentially to layer 1 than neurons of the ventral anterior-ventral lateral nuclear complex in the rat. Cereb. Cortex *25*, 221–235.

Kuriakose, R., Saha, U., Castillo, G., Udupa, K., Ni, Z., Gunraj, C., Mazzella, F., Hamani, C., Lang, A.E., Moro, E., et al. (2010). The nature and time course of cortical activation following subthalamic stimulation in parkinson's disease. Cereb. Cortex *20*, 1926–1936.

Labedi, A., Benali, A., Mix, A., Neubacher, U., and Funke, K. (2014). Modulation of Inhibitory Activity Markers by Intermittent Theta-burst Stimulation in Rat Cortex is NMDA-receptor Dependent. Brain Stimul. 2013.

Larkum, M.E., Senn, W., and Lüscher, H.R. (2004). Top-down dendritic input increases the gain of layer 5 pyramidal neurons. Cereb. Cortex *14*, 1059–1070.

Di Lazzaro, V., and Ziemann, U. (2013). The contribution of transcranial magnetic stimulation in the functional evaluation of microcircuits in human motor cortex. Front. Neural Circuits *7*, 18.

Di Lazzaro, V., Oliviero, A., Profice, P., Saturno, E., Pilato, F.,

Insola, A., Mazzone, P., Tonali, P., and Rothwell, J.C. (1998). Comparison of descending volleys evoked by transcranial magnetic and electric stimulation in conscious humans. Electroencephalogr. Clin. Neurophysiol. *109*, 397–401.

Di Lazzaro, V., Oliviero, A., Meglio, M., Cioni, B., Tamburrini, G., Tonali, P., and Rothwell, J.C. (2000). Direct demonstration of the effect of lorazepam on the excitability of the human motor cortex. Clin. Neurophysiol. *111*, 794–799.

Di Lazzaro, V., Oliviero, A., Saturno, E., Pilato, F., Insola, A., Mazzone, P., Profice, P., Tonali, P., and Rothwell, J.C. (2001). The effect on corticospinal volleys of reversing the direction of current induced in the motor cortex by transcranial magnetic stimulation. Exp. Brain Res. *138*, 268–273.

Di Lazzaro, V., Ziemann, U., and Lemon, R.N. (2008). State of the art: Physiology of transcranial motor cortex stimulation. Brain Stimul. *1*, 345–362.

Di Lazzaro, V., Profice, P., Ranieri, F., Capone, F., Dileone, M., Oliviero, A., and Pilato, F. (2012). I-wave origin and modulation. Brain Stimul. *5*, 512–525.

Lefaucheur, J., André-Obadia, N., Antal, A., Ayache, S.S., Baeken, C., Benninger, D.H., Cantello, R.M., Cincotta, M., de Carvalho, M., De Ridder, D., et al. (2014). Evidence-based guidelines on the therapeutic use of repetitive transcranial magnetic stimulation (rTMS). Clin. Neurophysiol. *125*, 2150–2206.

Liang, F., Rouiller, E.M., and Wiesendanger, M. (1993). Modulation of sustained electromyographic activity by single intracortical

microstimuli: comparison of two forelimb motor cortical areas of the rat. Somatosens. Mot. Res. *10*, 51–61.

Logothetis, N.K., Pauls, J., Augath, M., Trinath, T., and Oeltermann, A. (2001). Neurophysiological investigation of the basis of the fMRI signal. Nature *412*, 150–157.

Maccabee, P.J., Eberle, L., Amassian, V.E., Cracco, R.Q., Rudell, A., and Jayachandra, M. (1990). Spatial distribution of the electric field induced in volume by round and figure “8” magnetic coils: relevance to activation of sensory nerve fibers. Electroencephalogr. Clin. Neurophysiol. *76*, 131–141.

Makowiecki, K., Harvey, A.R., Sherrard, R.M., and Rodger, J. (2014). Low-Intensity Repetitive Transcranial Magnetic Stimulation Improves Abnormal Visual Cortical Circuit Topography and Upregulates BDNF in Mice. J. Neurosci. *34*, 10780–10792.

Malenka, R.C., and Bear, M.F. (2004). LTP and LTD: an embarrassment of riches. Neuron *44*, 5–21.

McDonnell, M.N., Orekhov, Y., and Ziemann, U. (2006). The role of GABA(B) receptors in intracortical inhibition in the human motor cortex. Exp. Brain Res. *173*, 86–93.

Mix, A., Benali, A., Eysel, U.T., and Funke, K. (2010). Continuous and intermittent transcranial magnetic theta burst stimulation modify tactile learning performance and cortical protein expression in the rat differently. Eur J Neurosci *32*, 1575–1586.

Moliadze, V., Zhao, Y., Eysel, U., and Funke, K. (2003). Effect of transcranial magnetic stimulation on single-unit activity in the cat primary visual cortex. J Physiol *553*, 665–679.

Moliadze, V., Giannikopoulos, D., Eysel, U.T., and Funke, K. (2005). Paired-pulse transcranial magnetic stimulation protocol applied to visual cortex of anaesthetized cat: effects on visually evoked single-unit activity. J. Physiol. *566*, 955–965.

Morishima, M., and Kawaguchi, Y. (2006). Recurrent connection patterns of corticostriatal pyramidal cells in frontal cortex. J. Neurosci. *26*, 4394–4405.

Morishima, M., Morita, K., Kubota, Y., and Kawaguchi, Y. (2011). Highly Differentiated Projection-Specific Cortical Subnetworks. J. Neurosci. *31*, 10380–10391.

Mueller, J.K., Grigsby, E.M., Prevosto, V., Petraglia, F.W., Rao, H., Deng, Z.-D., Peterchev, A. V, Sommer, M.A., Egner, T., Platt, M.L., et al. (2014). Simultaneous transcranial magnetic stimulation and single-neuron recording in alert non-human primates. Nat. Neurosci. *17*, 1130–1136.

Muller, P.A., Dhamne, S.C., Vahabzadeh-Hagh, A.M., Pascual-Leone, A., Jensen, F.E., and Rotenberg, A. (2014). Suppression of motor cortical excitability in anesthetized rats by low frequency repetitive transcranial magnetic stimulation. PLoS One *9*, e91065.

Murphy, S.C., Palmer, L.M., Nyffeler, T., Müri, R.M., and Larkum, M.E. (2016). Transcranial magnetic stimulation (TMS) inhibits cortical dendrites. Elife *5*, 1–12.

Nakamura, H., Kitagawa, H., Kawaguchi, Y., and Tsuji, H. (1996). Direct and indirect activation of human corticospinal neurons by transcranial magnetic and electrical stimulation. Neurosci. Lett. *210*, 45–48.

Nakamura, H., Kitagawa, H., Kawaguchi, Y., and Tsuji, H. (1997). Intracortical facilitation and inhibition after transcranial magnetic stimulation in conscious humans. J. Physiol. *498 (Pt 3*, 817–823.

Nakamura, K.C., Sharott, A., and Magill, P.J. (2014). Temporal coupling with cortex distinguishes spontaneous neuronal activities in identified basal ganglia-recipient and cerebellar-recipient zones of the motor thalamus. Cereb. Cortex *24*, 81–97.

Nambu, A., Tokuno, H., and Takada, M. (2002). Functional significance of the cortico–subthalamo–pallidal 'hyperdirect' pathway. Neurosci. Res. *43*, 111–117.

Nielsen, J.B., Perez, M.A., Oudega, M., Enriquez-Denton, M., and Aimonetti, J.-M. (2007). Evaluation of transcranial magnetic stimulation for investigating transmission in descending motor tracts in the rat. Eur. J. Neurosci. *25*, 805–814.

Oswald, M.J., Tantirigama, M.L.S., Sonntag, I., Hughes, S.M., and Empson, R.M. (2013). Diversity of layer 5 projection neurons in the mouse motor cortex. Front. Cell. Neurosci. *7*.

Pascual-Leone, A., Valls-Solé, J., Wassermann, E.M., and Hallett, M. (1994). Responses to rapid-rate transcranial magnetic stimulation of the human motor cortex. Brain *117*, 847–858.

Pasley, B.N., Allen, E.A., and Freeman, R.D. (2009). State-dependent variability of neuronal responses to transcranial magnetic stimulation of the visual cortex. Neuron *62*, 291–303.

Patton, H.D., and Amassian, V.E. (1954). Single and multiple-unit analysis of cortical stage of pyramidal tract activation. J. Neurophysiol. *17*, 345–363.

Paus, T., Jech, R., Thompson, C.J., Comeau, R., Peters, T., and Evans, a C. (1997). Transcranial magnetic stimulation during positron emission tomography: a new method for studying connectivity of the human cerebral cortex. J. Neurosci. *17*, 3178–3184.

Paxinos, G., and Watson, C. (2006). The Rat Brain in Stereotaxic Coordinates (Waltham, USA: Academic Press).

Percheron, G., François, C., Talbi, B., Yelnik, J., and Fénelon, G. (1996). The primate motor thalamus. Brain Res. Brain Res. Rev. *22*, 93–181.

Quiroga, R.Q., Nadasdy, Z., and Ben-Shaul, Y. (2004). Unsupervised spike detection and sorting with wavelets and superparamagnetic clustering. Neural Comput. *16*, 1661–1687.

R Core Team (2016). R: A language and environment for statistical computing. R Found. Stat. Comput.

Reis, J., Swayne, O.B., Vandermeeren, Y., Camus, M., Dimyan, M.A., Harris-Love, M., Perez, M.A., Ragert, P., Rothwell, J.C., and Cohen, L.G. (2008). Contribution of transcranial magnetic stimulation to the understanding of cortical mechanisms involved in motor control. J. Physiol. *586*, 325–351.

Rosanova, M., Casali, A.G., Bellina, V., Resta, F., Mariotti, M., and Massimini, M. (2009). Natural Frequencies of Human Corticothalamic Circuits. J. Neurosci. *29*, 7679–7685.

Rotenberg, A., Muller, P.A., Vahabzadeh-Hagh, A.M., Navarro, X., López-Vales, R., Pascual-Leone, A., and Jensen, F. (2010). Lateralization of forelimb motor evoked potentials by transcranial magnetic stimulation in rats. Clin. Neurophysiol. *121*, 104–108.

Rusu, C. V., Murakami, M., Ziemann, U., and Triesch, J. (2014). A model of TMS-induced I-waves in motor cortex. Brain Stimul. *7*, 401–414.

Sakai, K., Ugawa, Y., Terao, Y., Hanajima, R., Furubayashi, T., and Kanazawa, I. (1997). Preferential activation of different I waves by transcranial magnetic stimulation with a figure-of-eight-shaped coil. Exp. Brain Res. *113*, 24–32.

Scanziani, M., and Häusser, M. (2009). Electrophysiology in the age of light. Nature *461*, 930–939.

Shepherd, G.M.G. (2013). Corticostriatal connectivity and its role in disease. Nat. Rev. Neurosci. *14*, 278–291.

Sherman, S.M., and Guillery, R.W. (2006). Exploring the thalamus and its role in cortical function (MIT Press).

Shinoda, Y., Izawa, Y., Sugiuchi, Y., and Futami, T. (1997). Functional significance of excitatory projections from the precerebellar nuclei to interpositus and dentate nucleus neurons for mediating motor, premotor and parietal cortical inputs. Prog. Brain Res. *114*, 193–207.

Stetkarova, I., and Kofler, M. (2013). Differential effect of baclofen on cortical and spinal inhibitory circuits. Clin. Neurophysiol. *124*, 339–345.

Suppa, A., Huang, Y.-Z., Funke, K., Ridding, M.C., Cheeran, B., Di Lazzaro, V., Ziemann, U., and Rothwell, J.C. (2016). Ten years of theta burst stimulation in humans: established knowledge, unknowns and prospects. Brain Stimul. *9*, 323–335.

Tang, A.D., Lowe, A.S., Garrett, A.R., Woodward, R., Bennett, W., Canty, A.J., Garry, M.I., Hinder, M.R., Summers, J.J., Gersner, R.,

et al. (2016). Construction and Evaluation of Rodent-Specific rTMS Coils. Front. Neural Circuits *10*, 1–10.

The Magstim Company Ltd. (2018). Magstim Coils Catalog.

Thimm, A., and Funke, K. (2015). Multiple blocks of intermittent and continuous theta-burst stimulation applied via transcranial magnetic stimulation differently affect sensory responses in rat barrel cortex. J. Physiol. *593*, 967–985.

Tischler, H., Wolfus, S., Friedman, A., Perel, E., Pashut, T., Lavidor, M., Korngreen, A., Yeshurun, Y., and Bar-Gad, I. (2011). Mini-coil for magnetic stimulation in the behaving primate. J. Neurosci. Methods *194*, 242–251.

Tofts, P.S., and Branston, N.M. (1991). The measurement of electric field, and the influence of surface charge, in magnetic stimulation. Electroencephalogr. Clin. Neurophysiol. *81*, 238–239.

Tokimura, H., Ridding, M.C., Tokimura, Y., Amassian, V.E., and Rothwell, J.C. (1996). Short latency facilitation between pairs of threshold magnetic stimuli applied to human motor cortex. Electroencephalogr. Clin. Neurophysiol. - Electromyogr. Mot. Control *101*, 263–272.

Trippe, J., Mix, A., Aydin-Abidin, S., Funke, K., and Benali, A. (2009). θ burst and conventional low-frequency rTMS differentially affect GABAergic neurotransmission in the rat cortex. Exp. Brain Res. *199*, 411–421.

Valls-Solé, J., Pascual-Leone, A., Wassermann, E.M., and Hallett, M. (1992). Human motor evoked responses to paired transcranial magnetic stimuli. Electroencephalogr. Clin. Neurophysiol.

85, 355–364.

Wagner, T., Valero-Cabre, A., and Pascual-Leone, A. (2007). Noninvasive human brain stimulation. Annu. Rev. Biomed. Eng. *9*, 527–565.

Walsh, V., and Cowey, A. (2000). Transcranial magnetic stimulation and cognitive neuroscience. Nat. Rev. Neurosci. *1*, 73–79.

Ziemann, U., and Rothwell, J.C. (2000). I-waves in motor cortex. J. Clin. Neurophysiol. *17*, 397–405.

Ziemann, U., Rothwell, J.C., and Ridding, M.C. (1996). Interaction between intracortical inhibition and facilitation in human motor cortex. J. Physiol. *496*, 873–881.

Ziemann, U., Tergau, F., Wassermann, E.M., Wischer, S., Hildebrandt, J., and Paulus, W. (1998). Demonstration of facilitatory I wave interaction in the human motor cortex by paired transcranial magnetic stimulation. J. Physiol. *511*, 181–190.

7. Acknowledgement

This doctoral work would not be possible without the guidance and support given to me by many individuals.

I would like to first thank my doctoral advisors Dr. Alia Benali, Prof. Dr. Cornelius Schwarz, Prof. Dr. Martin Giese and Prof. Dr. Ulf Ziemann for their guidance, supervision, and technical and logistical support. I would also like to thank my collaborators Dr. Juha Virtanen and Axel Oeltermann for the collaboration on electronic development, which is of critical importance to this work. Furthermore, I'd like to thank Prof. Dr. Horst Herbert and the Graduate Training Centre/International Max Planck Research School for their continued support since the beginning of my master's study. Last but not least, I would like to thank my wife Ksenia and son Konstantin, as well as my parents Shuchun Li and Yueping Kong for their understanding, encouragement, and unconditional love.